

AN ABSTRACT OF THE THESIS OF

YEOUNG TING KAO for the Master of Science
(Name) (Degree)

in CIVIL ENGINEERING presented on 4 May 1973
(Major) (Date)

Title: CONSOLIDATION CHARACTERISTICS OF CALCAREOUS

DEEP SEA-FLOOR SEDIMENTS FROM THE PANAMA BASIN

Redacted for privacy

Abstract approved Dr. J. R. Bell

Calcareous sediments containing a large percentage of foraminiferal microskeletal tests were taken from sites in the Panama Basin and subjected to an investigation to determine the consolidation characteristics of this type of soil. The consolidation-stress curves and the time rate of consolidation curves in particular were investigated in this study.

The stress-volume characteristics during consolidation were found to vary according to the amount of particle crushing. Theoretical relationships were established between the compression index and void ratio or percentage of uncrushed tests. The validity of the theoretical approach was established by performing a laboratory investigation consisting of five consolidation tests, microscopic examinations and grain size analyses. The results of the laboratory investigation conformed to the theoretical interpretation of the relationship of compression index and void ratio. The five e -log p consolidation

curves were all concave downward showing the effects of crushing of foram particles. Further, the time rate of consolidation curves for these sediments were linear and may also be attributed to grain crushing.

Consolidation Characteristics of Calcareous Deep
Sea-Floor Sediments from the Panama Basin

by

Yeoung Ting Kao

A THESIS

submitted to

Oregon State University

in partial fulfillment of
the requirements for the
degree of

Master of Science

June 1974

APPROVED:

Redacted for privacy

Professor of ~~Civil~~ Engineering
in charge of major

Redacted for privacy

Head of Department of Civil Engineering

Redacted for privacy

Dean of Graduate School

Date thesis is presented 4 May 1973

Typed by Muriel Davis for Yeoung Ting Kao

ACKNOWLEDGMENTS

Deep gratefulness is owed to Dr. J. R. Bell who has been a constant inspiration. All the hours given for guidance, assistance, and improving of the manuscript will never be forgotten. Sincere appreciation is expressed to Dr. W. L. Schroeder for his constructive criticisms and for serving on my graduate advisory committee.

Many thanks to Mr. Gordon Beecroft for serving on my graduate advisory committee. Thanks also to Dr. Ted Moore for providing the microphotographs and to Dr. T. H. van Andel, who provided the sediment samples. Appreciation is expressed to the Office of Naval Research for financial support.

A very special thanks is expressed to my wife, Jeng-Ping, for her encouragement during the study and especially for the typing of the manuscript.

Throughout my entire academic career, I have received the most enthusiastic support from my parents. This thesis is dedicated to them.

TABLE OF CONTENTS

	<u>Page</u>
INTRODUCTION	1
THEORY	4
General	4
Degree of Crushing in Foram Particles	8
Void Ratio-Effective Stress Relationship	14
Time Rate of Consolidation Curves	21
LABORATORY STUDIES	24
Sampling	24
Apparatus and Procedure	25
TEST RESULTS	30
DISCUSSION OF RESULTS	40
CONCLUSIONS	54
RECOMMENDATIONS FOR FUTURE STUDY	56
BIBLIOGRAPHY	57

LIST OF FIGURES

<u>Figure</u>		<u>Page</u>
1	Stress-strain curves for confined compression	5
2	(a) Typical e-p curves. (b) Corresponding e-log p curves representing results of compression tests on laterally confined laboratory soil aggregates	7
3	Three conditions of the foram existence	9
4	The phases of an element of foram sediment	11
5	Compression diagrams	15
6	The void ratio vs log effective stress curve for the constant foram test and fragment contents	16
7	The void ratio vs log effective stress curve for the varying amount of the foram tests and fragments	16
8	The interpretation of the correlation between the compression index and void ratio	20
9	Time curve for a typical load increment on sand	22
10	Typical compression-time curve for high-stress test on sand	22
11	Effect of pressure on rate of secondary compression C_a	23
12	Location of samples	26
13	The equipment for preparation of sample	27
14	Consolidation equipment	28
15	Natural calcareous sediments	33
16	Foram particles retained on the sieve #100	33
17	Foram particles retained on the sieve #200	34

<u>Figure</u>		<u>Page</u>
18	Foram particles pass through the sieve #200	34
19	The void ratio vs log effective stress curves of Samples 12 at different depths	35
20	The void ratio vs log effective stress curves of Samples 19 and 23	36
21	The void ratio vs effective stress curves of Samples 19 and 23	35
22	Time rate of consolidation curves of Sample 19	38
23	Time rate of consolidation curves of Samples 23	39
24	Effective stress vs the rate of secondary compression curves	45
25	Effective stress-increment of the rate of secondary compression	46
26	The variation between apparent overconsolidation stress and depth (below ocean bottom)	48
27	The refined interpretation of the correlation between the compression index and void ratio	49
28	The relationship between the compression index and void ratio (from consolidation results)	51

LIST OF TERMS

<u>Term</u>	<u>Description</u>	<u>Dimensions</u>
C_a	rate of secondary compression	in/in
ΔC_a	increment of the rate of secondary compression	in/in
C_c	compression index for the foram sediments	dimensionless
C_{cf}	compression index for the foram fragments	"
C_{cm}	compression index for sand-clay mixture	"
C_{cp}	compression index for clay	"
D_e	external diameter of sphere	mm
D_i	internal diameter of sphere	mm
e	total void ratio	dimensionless
e_o	initial total void ratio	"
e_{in}	internal void ratio	"
e_{ino}	initial internal void ratio	"
e_{out}	external void ratio	"
F	fraction of nonclay material	percent
K	constant	dimensionless
P	consolidation stress	kg/cm^2
P'	effective stress	"
P'_c	apparent overconsolidation stress	"
P'_o	effective overburden stress	"

<u>Term</u>	<u>Description</u>	<u>Dimensions</u>
R	ratio of internal to external diameter	dimension- less
S_i	compression at initial point of the time rate of consolidation curves	in
V	total volume of voids	cm ³
ΔV	increment of void volume	"
V_o	initial total volume of voids	"
V_{in}	internal void volume	"
V_{ino}	initial internal void volume	"
V_{out}	external void volume	"
V_s	volume of solids	"
V'_s	the total volume of the hollow spheres in foram sediment	"
W	dry weight of the foram (whole) tests at any time	gm
W_s	dry weight of the total solids	"
$x\%$	the percentage of the foram test fraction	percent
σ_v	applied stress	lb/in ²

CONSOLIDATION CHARACTERISTICS OF CALCAREOUS
DEEP SEA-FLOOR SEDIMENTS
FROM THE PANAMA BASIN

INTRODUCTION

Following the improvement of the equipment and skill of drilling and sampling in the deep sea, many different kinds of soil tests and studies on the deep sea-floor sediments have been performed by numerous investigators. Only limited efforts, however, have been concerned with the engineering characteristics of deep sea-floor sediments. One of the most important areas requiring research is relative to consolidation characteristics. Information on these characteristics could be used to predict consolidation and settlement resulting from underwater foundations. Such information would also be valuable in geologic studies of sea floor sites.

Calcareous sediments cover wide areas on the deep sea floor. The sand size fraction of these sediments consist predominantly of microskeletal tests and fragments of the foraminiferids. These minute organisms are cream to white in color and composed mainly of nonplastic sand-to-silt-size particles which are hollow and crush easily. Influences of terrigenous clays make the calcareous samples exhibit different degrees of plasticity. Because of the tendency of the grains to crush, the calcareous sediments exhibit special consolidation characteristics. The bulk of the theories of stress-volume

relationships have been developed for clays. Only scattered information concerning the engineering behavior of deep sea-floor sediments containing significant amounts of hollow particles is available.

The purpose of this study was, therefore, to investigate the consolidation characteristics of calcareous sediments containing large percentages of skeletons of foraminifera. Special attention was to be given to the effects of grain crushing on the apparent overconsolidation stress, the shape of consolidation curves and secondary consolidation.

This thesis presents the results of a series of laboratory consolidation tests, sieve analyses, and microscopic examinations. Microphotographs were obtained showing the condition of individual foram particles and the natural calcareous sediments. Further, a theory has been developed to relate compression index to grain crushing. The tests were performed on samples from the Panama Basin which contained a very small percentage of clay.

The results of the laboratory study suggest that the consolidation of calcareous sediments tested was primarily due to the continuous crushing of foram tests and fragments. All the time rate of consolidation curves showed a linear relationship and the e -log p curves obtained were concave downward throughout the stress range tested. The results of the study indicated that for void ratios less than 2.19, the crushing of foram tests and fragments controlled the

system's behavior. In addition, a new method for finding the apparent overconsolidation stress in special sediments has been developed by plotting the increment of the rate of secondary compression versus consolidation stress. Based upon these values, a relationship between the apparent overconsolidation and the depth below the ocean bottom was obtained.

THEORY

General

The sediments of calcareous ooze mostly consist of micro-skeletal tests and fragments of the foraminiferids. These soils contain major components of sand-to-silt size particles which are hollow and crush easily. Consolidation is characteristic of particle crushing. So studies of basic theories of consolidation behavior relative to these sediments were concentrated on in the investigation of granular material with crushing properties.

The mechanism of compression (11) in a soil in which the cohesionless, organic, micaceous soil or sand is the major component, includes two parts. The first part is the bending and distortion of the grains which are largely elastic and in which compression is reversible. Fracture of the grains, particularly at their points of contact, is the second factor in the compression of these soils. This is not reversible. Lambe and Whitman (6) have investigated the stress-strain behavior of a medium to coarse uniform quartz sand during confined compression. They suggest that the stress strain behavior of sand should be considered in three stages.

1. For stresses up to about 2000 psi, the stress-strain curves are concave upward. Thus the sand gets stiffer and stiffer as the

level of stress increases. This form of stress-strain behavior, called locking, is very characteristic of particulate systems. The strains result primarily from the type of action shown in Figure 1 (a).

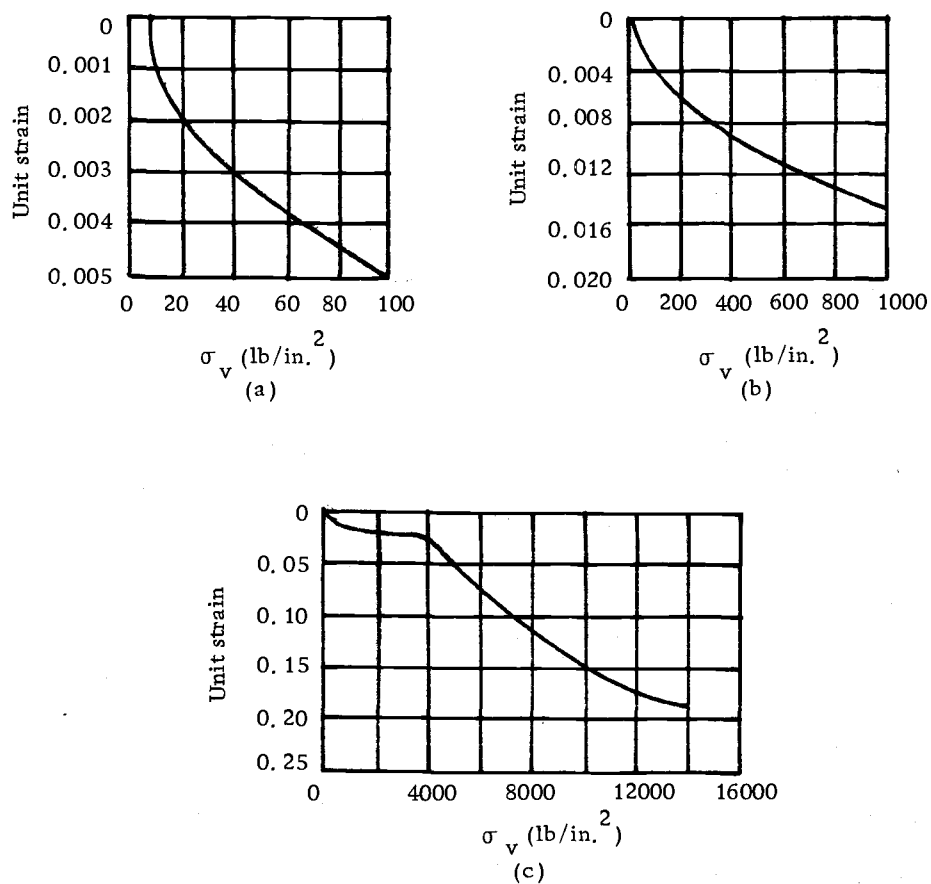


Figure 1. Stress-strain curves for confined compression. Ottawa sand, initial porosity = 0.375. (From Lambe and Whitman, 1969.)

As the stress is increased, first loose arrays within the soil will collapse, and then the denser arrays will. Each such movement results in a more tightly packed, hence stiffer, arrangement of particles. Finally, a stage is reached in which already dense arrays

are being squeezed more tightly together as contact points crush, thus allowing a little more sliding.

2. Starting at about 2000 psi, the stress-strain curve begins to develop a reverse curvature and becomes concave to the strain axis. This yielding is the result of fracturing of individual sand particles, which permits large relative motions between particles. Distinct popping sounds can be heard at this stage of loading. Microscopic examination and grain size analyses before and after testing show that considerable particle degradation actually occurs.

3. Fracturing the particles permits still tighter packing of the new and remaining particles. Since the number of particles has now increased, the average force per contact has actually decreased. Thus the sand once again becomes stiffer and stiffer as the stress increases still further.

These same general processes take place during the compression of all granular soils, although seldom in such distinct stages. Sliding between particles is usually present at all stress levels. Crushing and fracturing of particles actually begins in a minor way at very small stresses, but becomes increasingly important when some critical stress is reached. This critical stress is smaller when the particle size is large, the soil is loose, the particles are angular, the strength of the individual mineral particles is low, and the soil has a uniform gradation.

Gilboy (5) emphasized that the shape of the grain has a tremendous influence on the compression characteristics of a granular material. He found that the greater the proportion of flat grains in a granular mass, the greater the compressibility of the mass. Any system of soil classification which neglects the presence and the effect of scale-like particles is incomplete and erroneous. Terzaghi (13) refined Gilboy's curves as Figure 2. All of the e -log p curves have

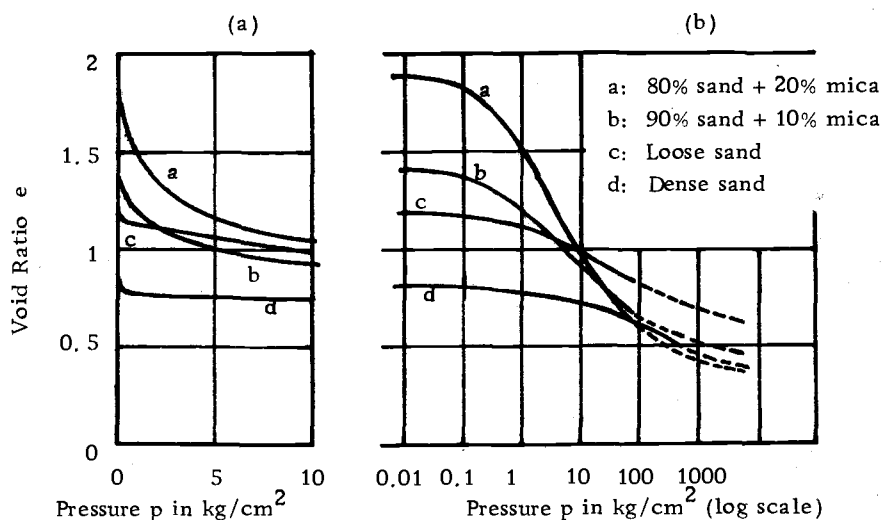


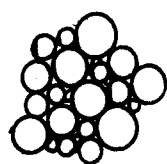
Figure 2. (a) Typical e - p curves. (b) Corresponding e -log p curves representing results of compression tests on laterally confined laboratory soil aggregates. (From Terzaghi and Peck, 1967).

certain characteristics in common. Each curve starts with a horizontal tangent and probably ends with a tangent that is nearly horizontal. The middle sloping part of each curve is fairly straight. Based upon these curves, the slopes of the straight line portions are apparently increasing with the increasing percentages of the mica

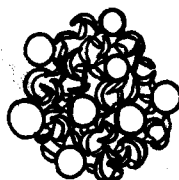
content (flat grains). Meanwhile, the apparent overconsolidation stress occurs earlier as a result of the increasing mica content. In foram soil, the whole skeletons could be considered as the sand particles and the fragments represent the scale-like particles.

Degree of Crushing in Foram Particles

There are four important factors which significantly influence the consolidation characteristics of the foram sediments: 1) initial void ratio, 2) scale-type particle content, 3) crushable foram tests content, and 4) clay content. For investigating the consolidation characteristics of foram sediments, the importance of the crushable tests content must be especially emphasized. Generally, foram particles exist in three conditions. First, the soil is simply composed of whole foram tests. Their voids have two aspects--internal void inside the test and external void outside the tests. Secondly, when pressure is applied to the sediment, foram tests start to crush and some foram fragments appeared in the soil. Water quickly dissipates out of a foram soil and is accompanied by a reduction of internal void volume. Thirdly, at high consolidation stress, all the foram tests respectively crush to overall fine fragments and there is no internal void volume (refer to Figure 3). The inside void ratio should, therefore, indicate the percentage of foram tests in the sediment.



Foram tests



Foram tests and fragments



Overall very fine fragments

Figure 3. Three conditions of the foram existence.

There are different physical properties for the foram tests and foram fragments. Tests exhibit a shell strength that resists compression, but foram fragments have only a small resistance to compression. The more fragments that exist, the more foram sediments will consolidate. However, there is some interaction between foram tests and fragments. When a foram test crushes, some internal voids will disappear instantaneously, and external voids will tend to increase by an equal amount; but the crushing of the test will be accompanied by the movement of other particles into a denser packing, and the overall void ratio will be decreased. Thus external voids can be assumed relatively constant throughout consolidation until all the tests have been crushed to fragments. Therefore, the changing of the total void ratio (e) is equal to the reduction of internal void ratio (e_{in}).

For determining the void ratio at which the granular particles contact, a rhombohedral system is assumed. Each sphere of the

next rhombic layer is placed in the hollow formed by three spheres of the lower layer. Faroueki and Winterkorn (4) have indicated that the rhombohedral system is the most important theoretically, and is usually the basis for calculations. Based upon this system, the void ratio of the uniform spheres was found to be 0.35. Foram particles possessed a smaller void ratio than 0.35 because of the different sizes of spheres occurring in the soil. In the rhombohedral system, a fine to coarse sand contained a minimum void ratio of 0.20 (6). Because foram sediments are more uniform than a fine to coarse sand, a foram soil should have a larger void ratio than 0.20. In summary, foram tests, each composed of three or four spherical bodies of equal size, make up foram sediments which may have the equivalent average void ratio, 0.275, of the above values. This value is for solid particles, but foram tests are hollow. To relate the various volumes for such particles it is necessary to know the ratio of internal to external diameter, R , of the particles. By being particulate, an element of foram soil is inherently multiphase. A typical element of foram soil contains two distinct components, foram shells and voids. A typical element is separated into phases as shown in Figure 4.

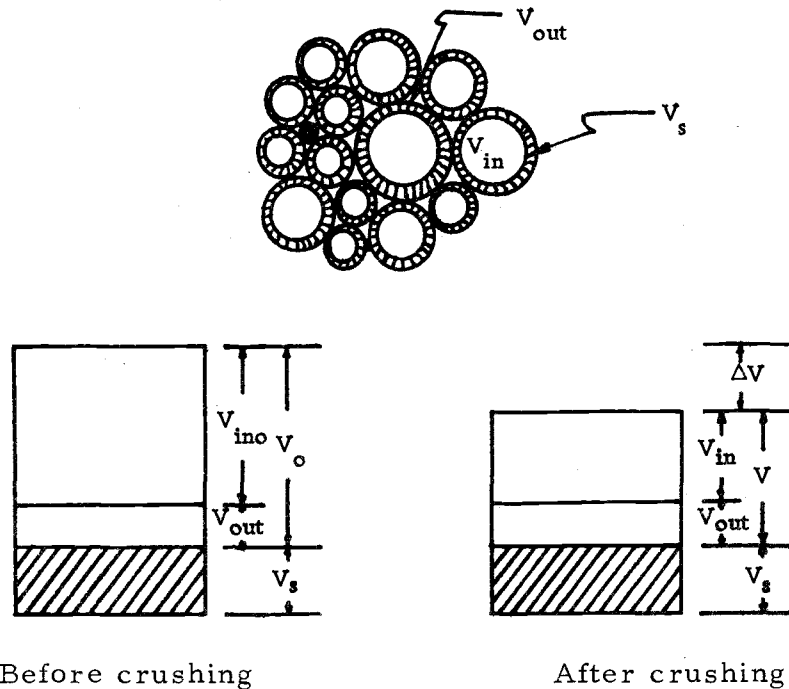


Figure 4. The phases of an element of foram sediment.

The initial internal void ratio, e_{ino} , and the initial total void ratio, e_o , can be determined for a rhombohedral system of hollow spheres from the following equations:

$$e_{ino} = \frac{V_{ino}}{V_s} = \frac{\text{initial internal void volume}}{\text{volume of solids}}$$

$$R = \frac{D_i}{D_e} = \frac{\text{internal diameter of sphere}}{\text{external diameter of sphere}}$$

$$\text{then } e_{ino} = \frac{\pi/6 D_e^3 R^3}{\pi/6 D_e^3 (1-R^3)} = \frac{R^3}{1-R^3} \quad (1)$$

$$\text{and } e_o = \frac{\text{initial total void volume}}{\text{volume of solids}}$$

$V = V_{ino} + V_{out}$ where V_{out} is the void volume outside the spheres.

V_{out} is assumed constant.

Since initial external void ratio, e_{out} , is equal to 0.275 for solid spheres

$$e_{out} = 0.275 = \frac{V_{out}}{V'_s}$$

where V'_s equals the total volume of the sphere and therefore,

$$V'_s = V_s + V_{ino}$$

Now

$$e_o = \frac{V_{ino} + 0.275 (V_s + V_{ino})}{V_s}$$

and

$$e_o = 0.275 + 1.275 \frac{V_{ino}}{V_s} = 0.275 + 1.275 e_{ino}$$

Combining with equation (1)

$$e_o = 0.275 + 1.275 \left(\frac{R^3}{1-R^3} \right) \quad (2)$$

Also, since $e_o = e_{ino} + e_{out}$

$$e_{out} = \frac{0.275}{1-R^3} \quad (3)$$

Based upon the assumption mentioned before, the change of the foram test content could be represented by the volume change of internal voids. The percentage of the foram test fraction ($x\%$) could also be regarded as the ratio of the internal void volume (V_{in}) at any

time of the consolidation to the initial internal void volume (V_{ino}).

Considering the void ratio changes, a development of the relationship between the foram test content and void ratio is as follows.

The percentage of tests ($x\%$) is the dry weight (W) of the whole tests at any time relative to the dry weight (W_s) of the total solids in the rhombohedral system described previously.

$$x\% = \frac{W}{W_s} (100) \quad (4)$$

For the hollow spheres, this is also equal to the ratio of the internal void volumes and hence to the internal void ratios.

$$x\% = \frac{V_{in}}{V_{ino}} (100) = \frac{e_{in}}{e_{ino}} (100)$$

Letting $\Delta e = e_o - e$ and for e_{out} a constant

$$\Delta e = (e_{ino} + e_{out}) - (e_{in} + e_{out}) = e_{ino} - e_{in} = \Delta e_{in}$$

thence,

$$x\% = \frac{e_{ino} - \Delta e_{in}}{e_{ino}} (100) = \frac{e_{ino} - (e_o - e)}{e_{ino}} (100)$$

and

$$x\% = \frac{e - (e_o - e_{ino})}{e_{ino}} (100) = \frac{e - e_{out}}{e_{ino}} (100)$$

Substitute e_{out} and e_{ino} values. Finally

$$x\% = \frac{e - \left(\frac{0.275}{3}\right)}{\left(\frac{R}{3}\right)} (100) \quad (5)$$

$$x\% = \frac{1 - R}{1 - R^3} (100)$$

Void Ratio-Effective Stress Relationship (e-log p curves)

Sand possesses somewhat similar crushing properties as foram particles. Two distinct stages occur on each e-log p curve as shown in Figure 5 (9). Above an apparent overconsolidation stress, sand particles only undergo small amounts of crushing. Each e-log p curve above the apparent overconsolidation stress has a flat relatively straight line. If most sand will not crush even at very high consolidation stress, the e-log p curve will keep a flat straight line throughout the consolidation test. As the apparent overconsolidation stress is exceeded, the sand starts to crush and the e-log p curves become a steep straight line. In other words, if there is no critical stress above which crushing is slight, the overall crushing will begin at the initial loading and the e-log p curve would be a straight line throughout the consolidation test.

With foram particles, the crushing of foram tests and fragments will influence the compression index. If foram tests remain constant, the compression is only due to the continuous crushing of the fragments. Thus, the e-log p curve is more or less a straight line with a constant compression index (refer to Figure 6). Besides the simple crushing of the fragments, the amount of fragments is also increasingly produced by the crushing of foram tests. So the compression index will increase, and the e-log p curve will be concave downward (refer to Figure 7).

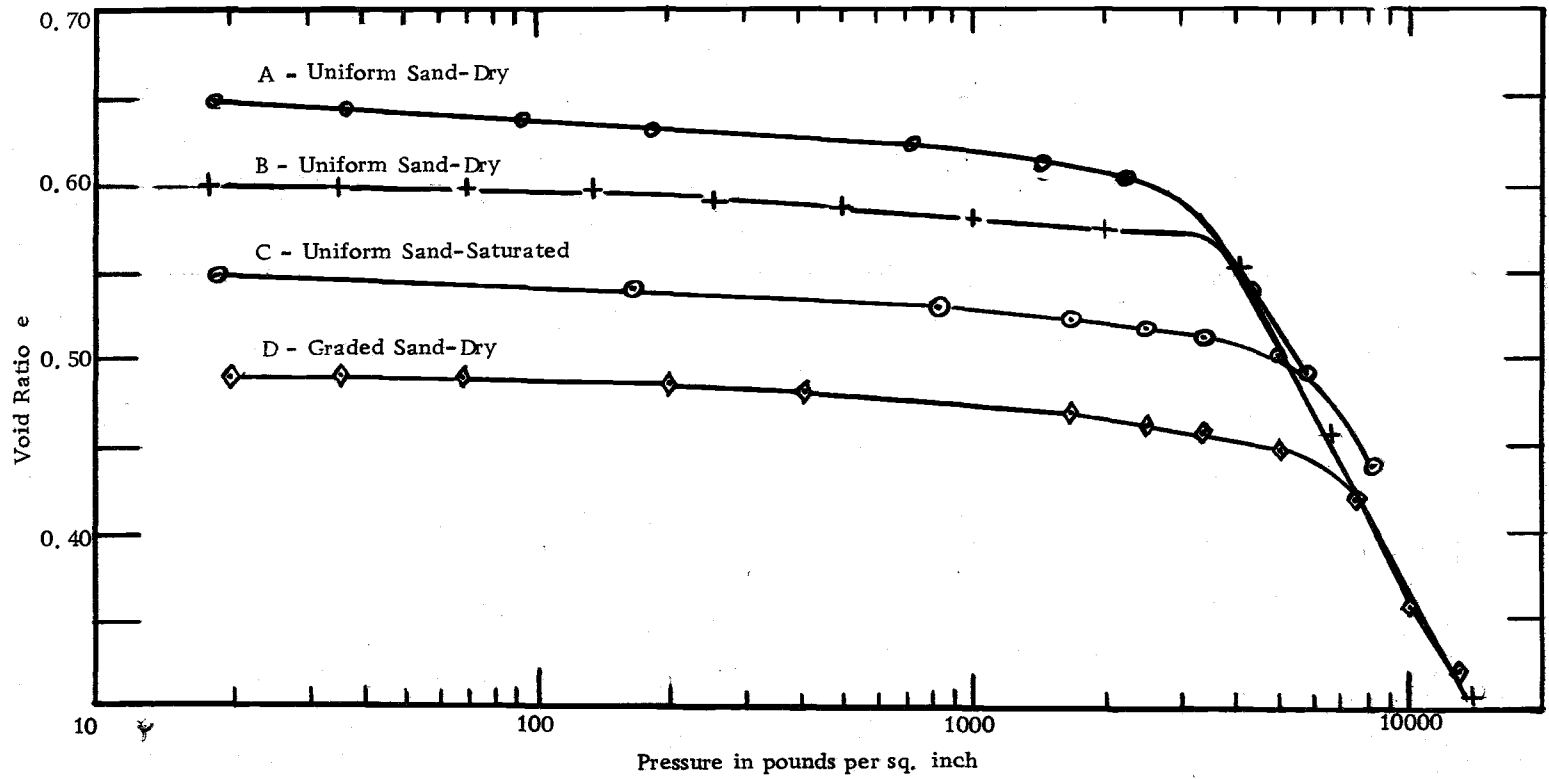


Figure 5. Compression diagrams (from J. E. Roberts and J. M. de Souza, 1958)

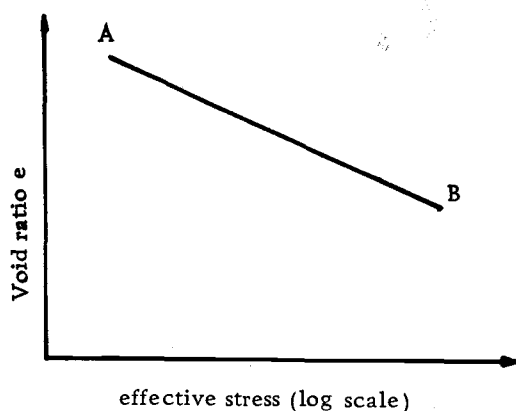


Figure 6. The void ratio vs log effective stress curve for the constant foram test and fragment contents.

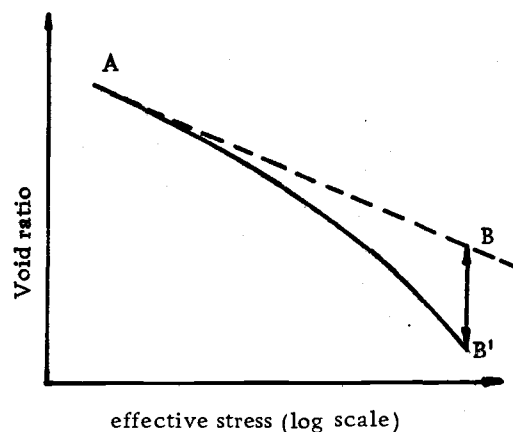


Figure 7. The void ratio vs log effective stress curve for the varying amount of the foram tests and fragments.

Each point on the e -log p curve represents a specific percentage of foram tests contained in the soil and the slope at that point is equal to the compression index for that percentage of foram tests. Based upon the above demonstration, the compression index at each individual point on the e -log p curve should be related to the void ratio which in turn is related to the percentage of whole tests by Equation 5. These values will be used to prepare a compression index-void ratio curve.

An investigation of the consolidation characteristics of sand-clay mixtures has been conducted by Anderson (3). He used different percentages of sand mixed with clay to find the corresponding compression index for each sample. A linear equation of the correlation between the compression index of a mixture (C_{cm}) and the fraction of nonclay material (F) was established as follows:

$$C_{cm} = \left(\frac{100-F}{100}\right) C_{cp}$$

where C_{cp} is the compression index of 100 percent clay (0 percent sand). But in foram particles, there is interaction between foram tests and fragments. The percentage of tests is gradually reduced throughout the consolidation and the percentage of fragments are, therefore, increased. The different proportions used in the sand-clay mixtures are automatically changed in a foram sample during testing. So an equation similar to the one above may also be used for describing the inter-relationship between the changing compression index and the decreasing percentage of tests existing in a foram sample.

$$C_c = \left(\frac{100-x\%}{100}\right) C_{cf} \quad (6)$$

The compression index changes everywhere on the e - $\log p$ curve of foram soil until all of the tests crush into fragments, and a short straight line on the e - $\log p$ curve would result. During that period, an unchanged compression index C_{cf} could be found. After substituting Equation (5) into Equation (6), a linear relationship between the compression index and the changing void ratio in foram particles is found as Equation (7).

$$C_c = \left(1 - \frac{e - \left(\frac{0.275}{3}\right)}{\left(\frac{R}{1-R^3}\right)}\right) C_{cf} \quad (7)$$

$$\text{or } C_c = \left(\frac{e_o - e}{e_{ino}} \right) C_{cf} \quad (8)$$

During consolidation, every foram sample will produce the same final fragmented form which will probably have the same C_{cf} value. After performing a series of lab tests on selected foram sediments, a final compression index C_{cf} can be found. Probably some foram samples would deviate from the compression index C_{cf} , because of different clay content. But by considering the factor of clay content, a corresponding C_{cf} should be obtained after performing a correction process.

In sand-clay mixtures, the proportion of clay minerals required to control soil behavior has been investigated. The Public Roads Administration presented a classification system in 1928 (8). The minimum percentage of coarse material required for subgrade stability was 65 percent. The Unified Soil Classification System (8) indicated that if more than 50 percent fine particles it belongs to a fine grained material. Murdock (7.) has conducted a consolidation investigation on gravel-clay mixtures. The compression index was found to become zero at 71 percent gravel. The mixtures were all assumed to be composed of a clay fraction and a nonclay fraction. The two components were assumed not to interact. But in foram particles interaction occurred between coarse foram tests and fine fragments, and there appears to be no distinct boundary between these two

components. Perhaps a transition zone exists between them. Based upon the findings on the sand-clay or gravel-clay mixtures, the lower and upper limits are probably between 50 percent and 71 percent of foram tests content. Above the upper limit, foram tests will dominate the soil behavior; below the lower limit, the magnitude of volume change for a stress increment will be a function of the compressibility of the fragments.

Furthermore, for the consolidation of foram sediments, it is interpreted that there are three ranges for the relationship between the compression index and the void ratio (refer to Figure 8). The first range is located from point A to point B, in which point A has an initial void ratio (e_0). Within this range, there may be at least 71 percent foram tests in soils, and volume change is controlled by the behavior of the foram tests. The elastic deformation of foram tests causes a slight change in the void ratio which defines a compression index, but the magnitude of the volume change for the foram tests is so small that it could be considered zero. Second range is found from point B to point C. In this transition zone, although foram tests still control soil behavior, the influence on the consolidation characteristics by the scale-like fragments becomes more significant. If there is some bonding stress or cementation among the particles it will progressively become relaxed during this period until the particles are completely free from its influence at point C. The compression

index and void ratio have a straight line relationship

$$C_c = K(e_B - e) \quad (9)$$

The third range is the main region which is between point C and point D. At point C the sediment contains about 50 percent foram tests, whereas at point D the sediment contains no whole foram tests. In this range the crushing of fragments mostly affects soil behavior. The relationship of the compression index C_c and void ratio is a straight line which extends to pass through origin point A. The relationship in this range has been indicated in Equation (8). After the third range has been exceeded, all the foram tests have been crushed to fragments. The internal void ratio becomes zero. The volume change is simply the result of the decrease of the external void ratio. Therefore, the uniform crush and rearrangement of fragments are characteristics of the foram materials. The compression index of uniform fragments may become constant, but this region is beyond the scope of this research.

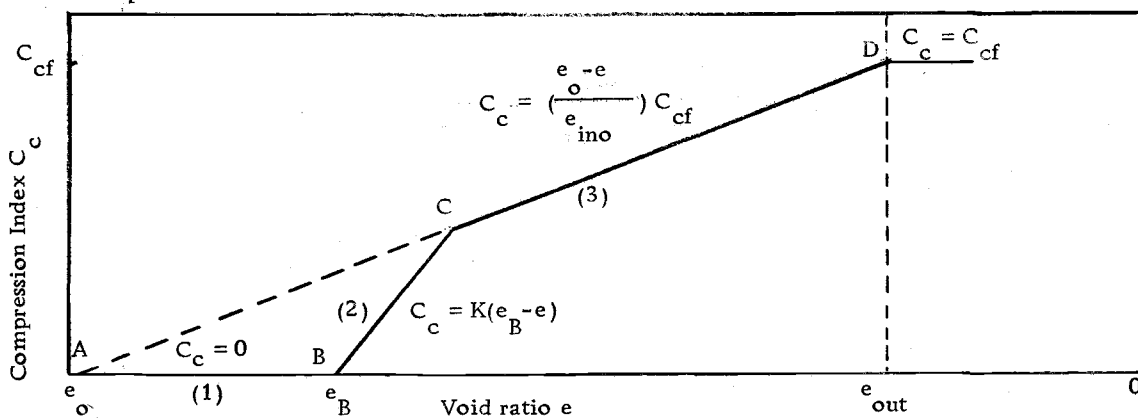


Figure 8. The interpretation of the correlation between the compression index and void ratio.

Time Rate of Consolidation Curves

Another phenomenon also is of special interest in connection with the compressibility of soils in general. It is the time rate at which the compression takes place. It can be divided into three stages (11): initial, primary and secondary. The initial stage occurs as soon as the load is applied. It occurs largely by the compression and solution of air in the soil voids. The primary compression is controlled by the escape of water from the soil voids. After the excess hydrostatic pressure had been dissipated, the compression may not cease. Instead it may continue indefinitely at an ever-decreasing rate. This is secondary compression. It appears to be the result of a plastic readjustment of the soil grains to the new stresses, of progressive fracture of the interparticle bonds, and possibility of progressive fracture of the particles themselves.

Based upon the test data from the consolidation of sand (9), the evidence suggests that at low pressure the importance of the time lag, which is due essentially to a continuous rearrangement of particles, depends on the initial density of the sample. Taylor (12) presents a time curve for a typical load increment on a uniform fairly dense sand in which about 95 percent of the total compression occurred during the first minute. (refer to Figure 9.) Roberts and de Souza (9) present a time curve for a compression test on a loose sand in which the

pressure was increased at a fairly rapid rate and then held constant at 6 kg/cm^2 . Even after one hour, the curve presented indicates the measurable compression was still occurring, as shown in Figure 10.

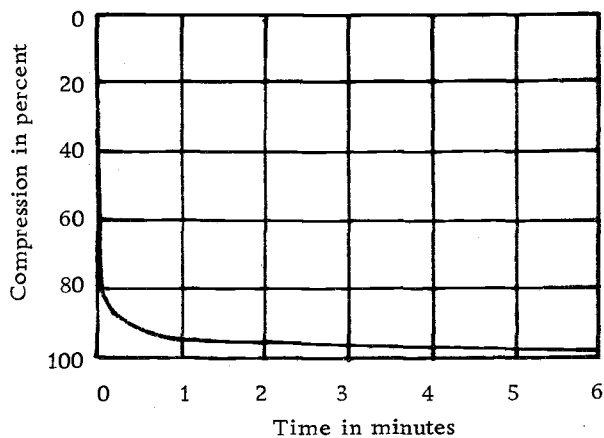


Figure 9. Time curve for a typical load increment on sand (from Taylor, 1948).

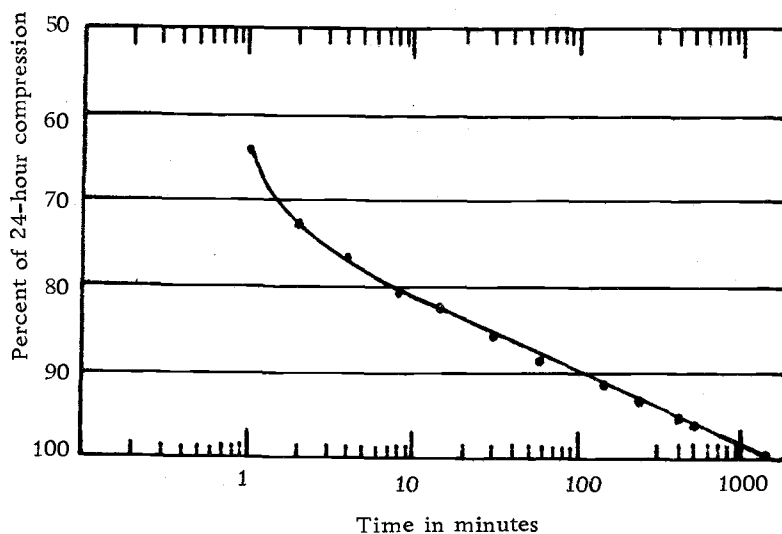


Figure 10. Typical compression-time curve for high-stress test on sand (from Roberts and deSouza, 1958).

Once the gross stress on the sample reaches or exceeds the apparent overconsolidated stress, the time lags during compression become more important. Generally, the time lag is due to a

continuing process: there is a gradual build-up of stress on individual grains resulting in shattering, a redistribution of stress occurs followed by a stress build-up and a shattering of other grains.

Singh and Yang (10) have investigated the secondary compression characteristics of a deep ocean sediment. They indicated that at low effective stresses the value of rate of secondary compression (C_a) is much smaller than at higher effective pressure. The value (C_a) increases with pressure to a maximum value and then decreases with higher pressures. The peak value occurred at a value slightly higher than the apparent preconsolidation pressure (refer to Figure 11). Here the rate of secondary compression (C_a) is a ratio in which the change in strain in the secondary region is divided by the corresponding change in the log of consolidation time.

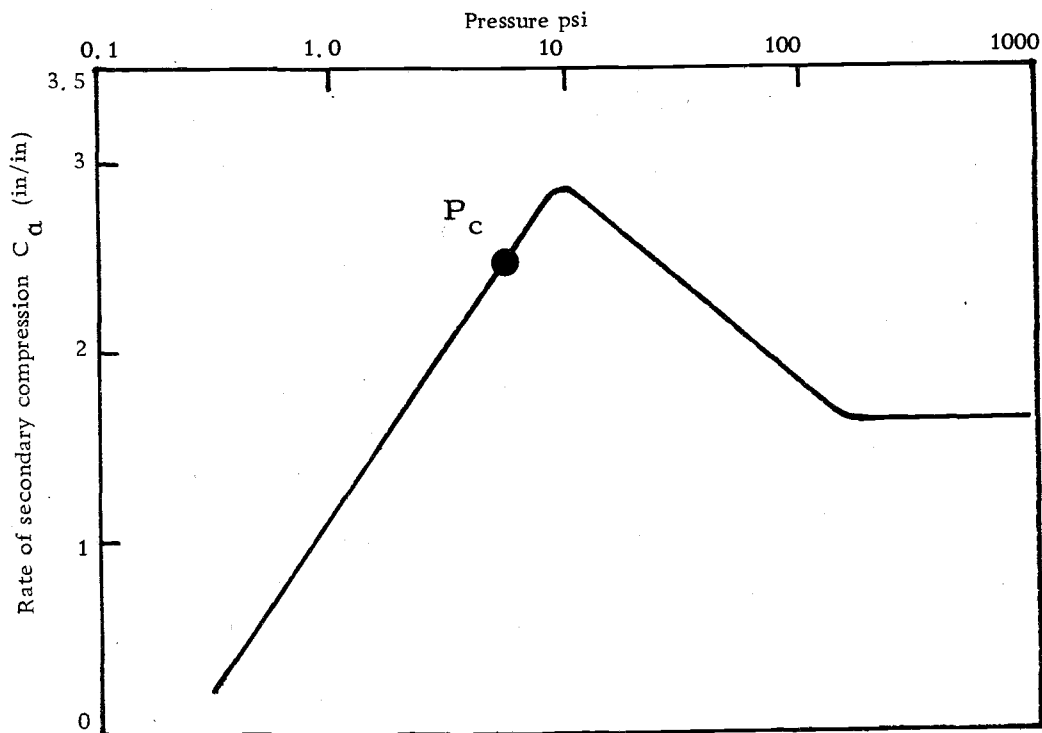


Figure 11. Effect of pressure on rate of secondary compression C_a (from A. Singh and Zen Yang, 1971).

LABORATORY STUDIES

Sampling

Five calcareous samples were taken from three selected locations on the Carnegie Ridge of the Panama Basin for this study of soil consolidation characteristics. Refer to the site location map, Figure 12. The samples were taken from a depth of approximately 2400 m, well above the compensation depth of 3400 m. Three samples were taken from core 12 and marked according to depth (in centimeters) as 12/135, 12/446, and 12/912. These soils were classified from light green to white ooze. Sample 19, from a depth of 877 cm, belonged to a light tan foram ooze. Sample 23, from a depth of 405 cm, was a greenish-tan foram ooze. In order to obtain corresponding data, all sample locations were selected as close as possible. To detect the relationship between depth and apparent overconsolidation stress, the samples used were taken from different depth below the ocean floor. These deep sea sediment samples were obtained with a piston sampler, which has a plastic liner with an external diameter of 2.5 inches, and a tube thickness of 1/8 inch. After the samples had been transported to the laboratory they were sealed in wax. Then they were stored in a refrigerator with a constant temperature of 20°C. All samples may have had some disturbance because of their high

sensitivity and their soft consistency.

Apparatus and Procedure

A series of tests were performed to define the sediment index properties. These laboratory tests were used to determine natural water content, specific gravity, plastic limit, liquid limit, and grain size distribution. Standard methods and apparatus for testing soils for the above determinations have been established by the American Society for Testing and Materials (2) and the American Association of State Highway Officials (1). Because of the hollow shape of foram particles, extra de-airing was necessary to remove trapped air before specific gravity could be determined accurately. The 50 ml pycnometer containing foram particles was left in a vacuum for approximately four hours.

Besides the standard general equipment used in a one-dimensional consolidation test, there was also a need for some special equipment such as a device for placing the specimen into a container, and a consolidation ring with a height of 2.4 cm and a diameter of 5.06 cm. In addition, a small trimming frame had to be designed which included a small jack and two round steel cylinders for pushing the soil sample out of the tube, as seen in Figure 13.

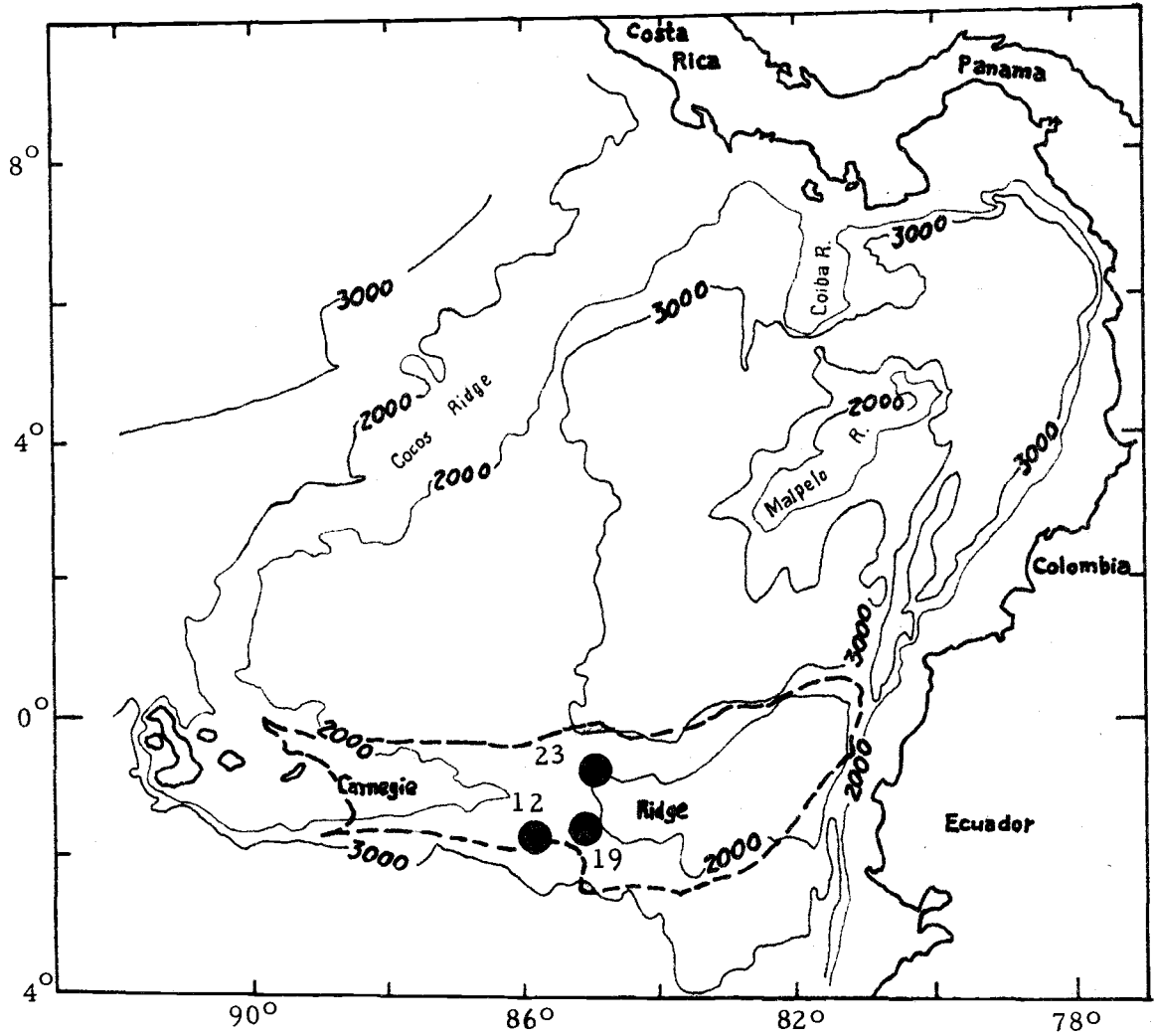


Figure 12. Location of samples.



Figure 13. The equipment for preparation of sample.

Because of the very low pressures involved in the test, a special loading system which was capable of transmitting a pressure as low as 0.0125 kg/cm^2 was designed and constructed. This equipment is shown in Figure 14. It consists of a number of thin lead plates of different weights, and the Conbel consolidometer.

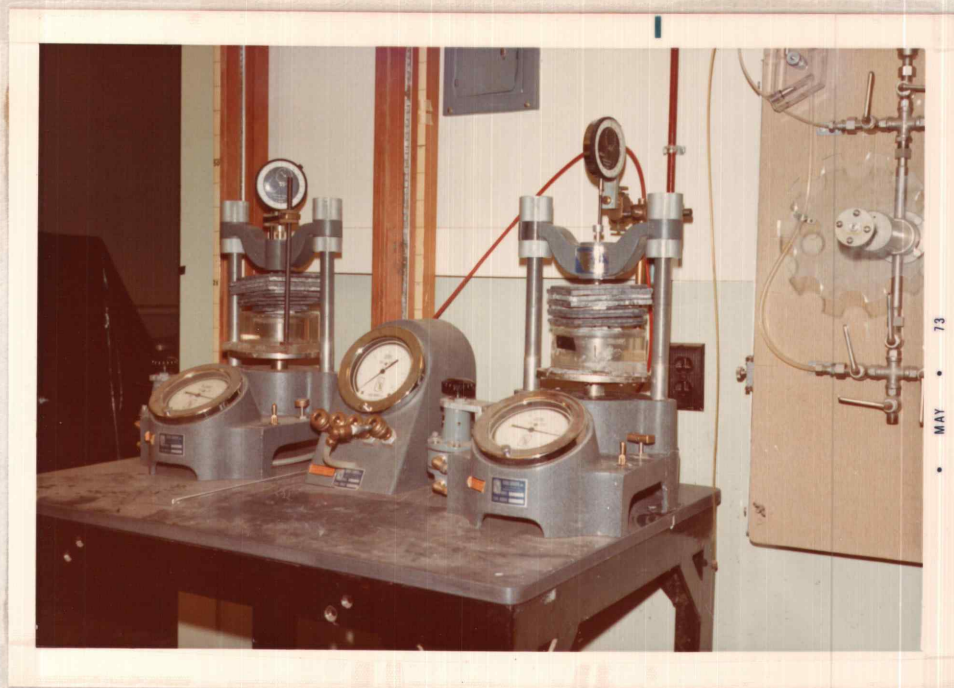


Figure 14. Consolidation equipment.

Three tests were conducted in a manner comparable to the normal consolidation test procedure. A load increment ratio ($\frac{\Delta P}{P}$) of approximately unit was used. Two more tests were performed using the load increment ratios two and three for investigating the effects of different load increment ratios on the time rate of consolidation. Also in order to find the effects of time, the time interval allowed for compression ranged from one day to five days. Initial time readings were taken as soon as possible within the first few seconds of loading. Sea water was used in the test to maintain the same soil salinity as in the deep sea.

After the test sample was prepared, the initial weights of the

ring and specimen were recorded. A pair of saturated porous discs were fitted to the top and bottom of the specimen before the assemblage was placed in a lucite dish. The dish was covered with a plastic bag to prevent evaporation. Then the loading head was positioned above the sample and the dial micrometer set.

Loading began with a low pressure of 0.0125 kg/cm^2 and terminated at different pressures for different samples: 51.2 kg/cm^2 for Samples 19 and 23, between 6 kg/cm^2 and 7 kg/cm^2 for Samples 12/135 and 12/912, and at 3 kg/cm^2 for Sample 12/446. The lead plates for each sample were selected according to a load increment ratio until the consolidation stress 0.8 kg/cm^2 was reached. Then the Conbel consolidometer started to work. The dial readings were taken to ± 0.0001 inches. After loading to the maximum desired pressure had been completed, the consolidometer was accordingly unloaded to 0.8 kg/cm^2 , 0.1 kg/cm^2 and 0.0125 kg/cm^2 . At the completion of each test, the sample was removed and weighed. Then, after the soil had been oven-dried, the initial water content was determined.

TEST RESULTS

The results of laboratory tests on the index properties of calcareous sediments are summarized in Table 1. Data included are sample number, depth, unit weight, initial void ratio, specific gravity, liquid limit, plastic limit, plasticity index, and natural water content. In spite of many carefully repeated tests, the plastic limit in Sample 23 still could not be found. In Sample 19 it almost approaches zero. Some material was taken from Samples 23 and 19 before and after consolidation tests for use in sieve analysis and microscopic examination. Table 2 shows the results of these sieve analyses. There are four representative microphotographs which have a magnification of 38. These pictures clearly indicate the condition of individual foram particles and the natural sediments (refer to Figures 15 to 18).

The void ratio-log effective stress curves for five samples are presented in Figures 19 and 20. Because of careless operation on the consolidation of Sample 12/912, the foram particles in the soil were crushed by applying a high consolidation stress at the beginning of the test. Thus it shows a very flat curve, and a low initial void ratio was obtained. Apparent overconsolidation appears in most curves except that of the disturbed sample. A straight line portion has not shown up on any void ratio-log effective stress curve. These curves tend to reach the same slope under high consolidation

Table 1. Index Properties of Calcareous Samples (Panama Basin)

Sample Number	Sample Depth (cm.)	Unit Weight g/cm^3	Initial Void Ratio e	Grain Specific Gravity GS	Liquid Limit (%)	Plastic Limit (%)	Plasticity Index (%)	Natural Water Content (%)
12	135	1.4	3.22	2.60	--	--	--	119
12	912	1.5	2.38	2.58	70	54.5	15.5	91
12	446	1.4	3.16	2.58	--	--	--	125
23	405	1.5	2.82	2.71	62	NP	NP	104
19	877	1.5	2.71	2.60	62	60	2	107

Table 2. Sieve Analysis Before and After the Consolidation of Samples 23 and 19 (in percent)

Sieve Analysis Section	Sample 23			Sample 19		
	Particles Retained on #100	Particles Retained on #200	Particles Pass through #200	Particles Retained on #100	Particles Retained on #200	Particles Pass through #200
Before consolidation	32.6	38.5	28.9	10.5	55.8	33.7
After consolidation	8.5	9.9	81.6	8.2	10.3	81.5
Changing amount	-24.1	-28.6	+52.7	-2.3	-45.5	+47.8

stress. The curves for Samples 23 and 19, especially, have a very similar shape.

Continuing further into the investigation of consolidation characteristics, Samples 19 and 23 were chosen to plot the void ratio vs. effective stress curves (Figure 21) and the time rate of consolidation curves (refer to Figures 22 and 23). There is a linear relationship between compression and time (log scale), even though the elapsed times and increment loading ratios are different.



Figure 15. Natural calcareous sediments.

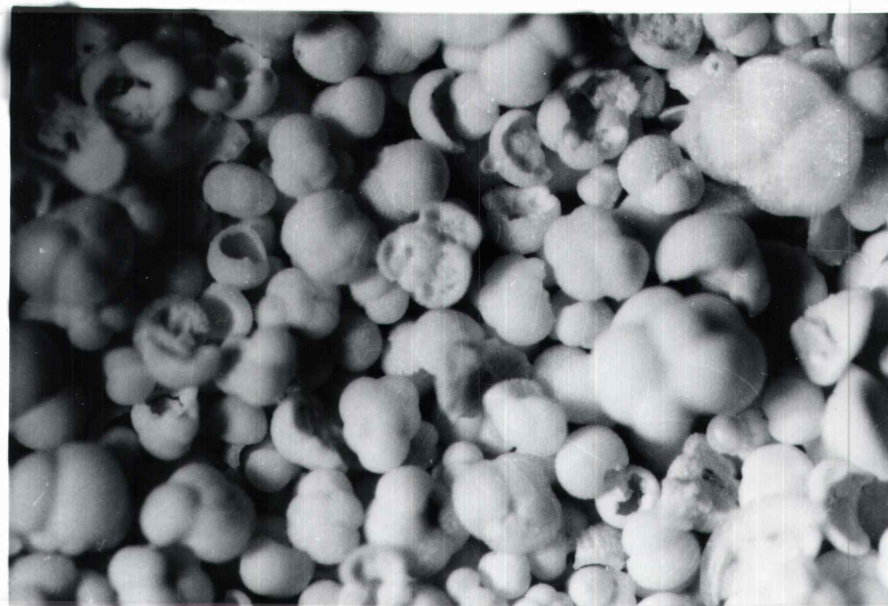


Figure 16. Foram particles retained on the sieve #100

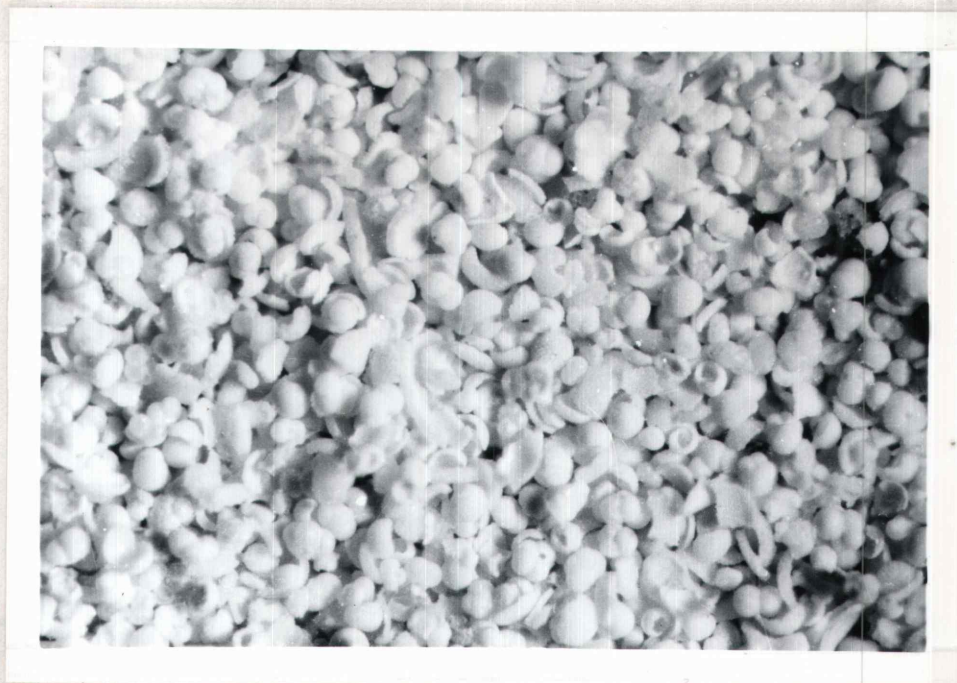


Figure 17. Foram particles retained on the sieve #200.



Figure 18. Foram particles pass through the sieve #200.

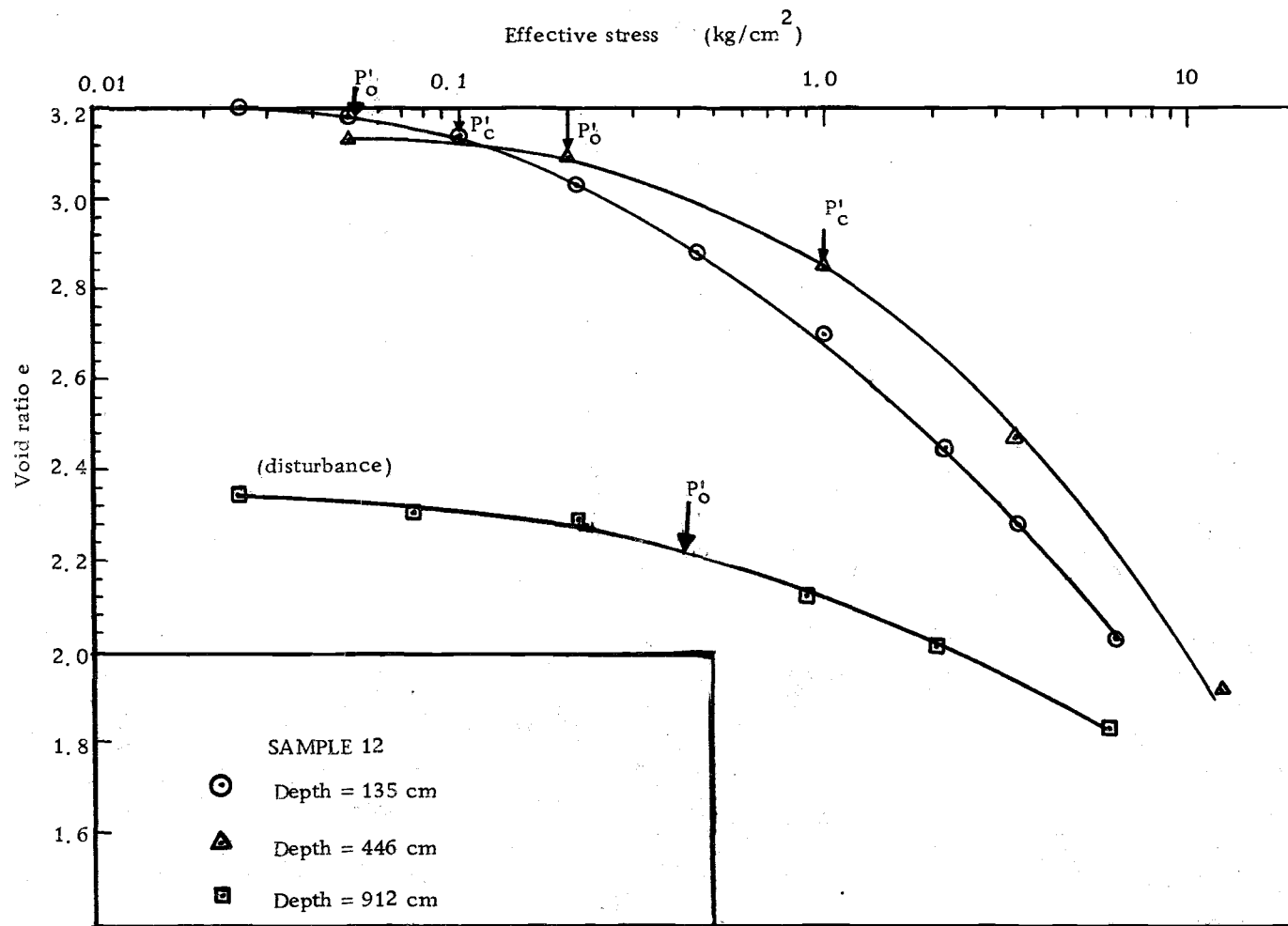


Figure 19. The void ratio vs log effective stress curves of Samples 12 at different depths.

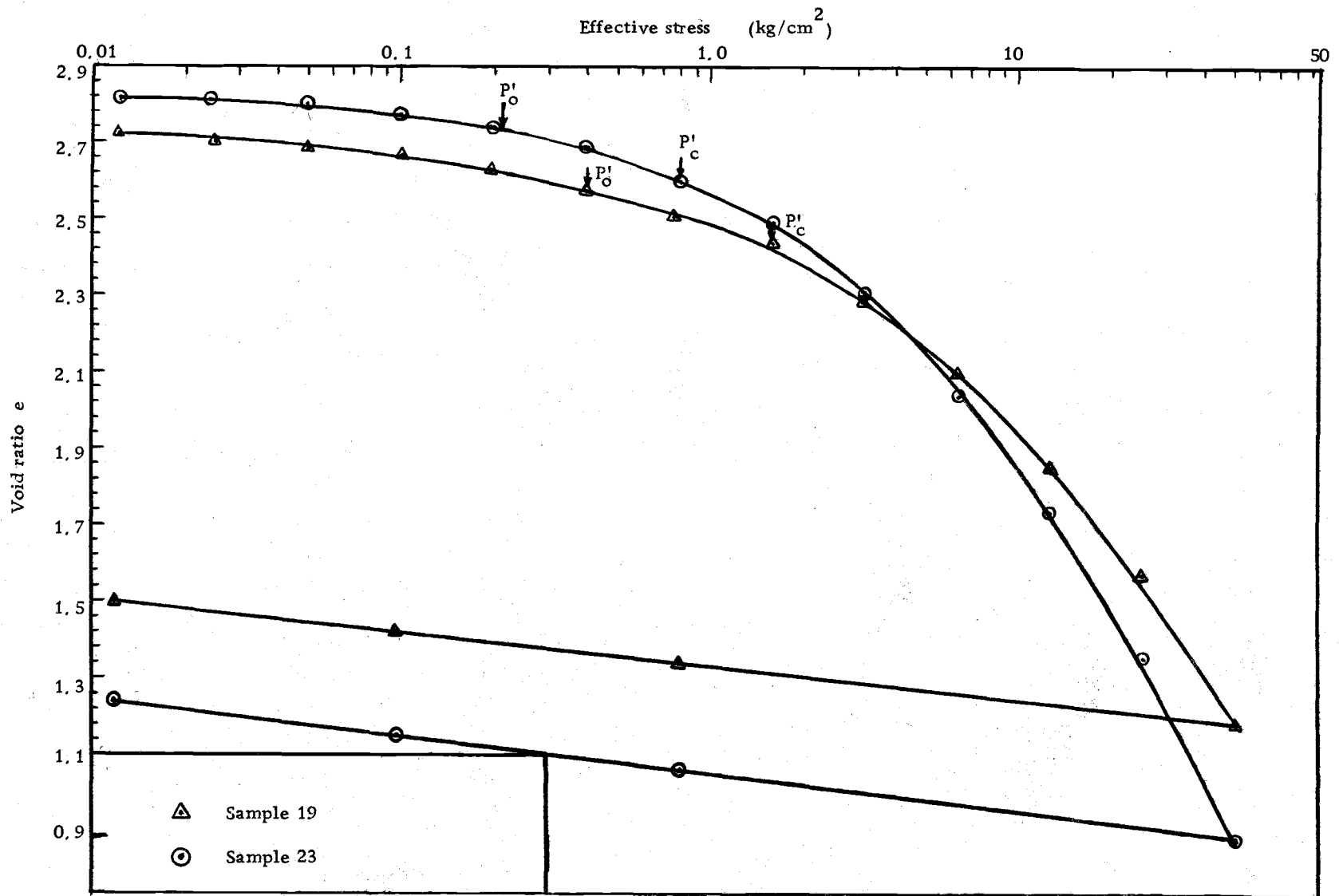


Figure 20. The void ratio vs log effective stress curves of Samples 19 and 23.

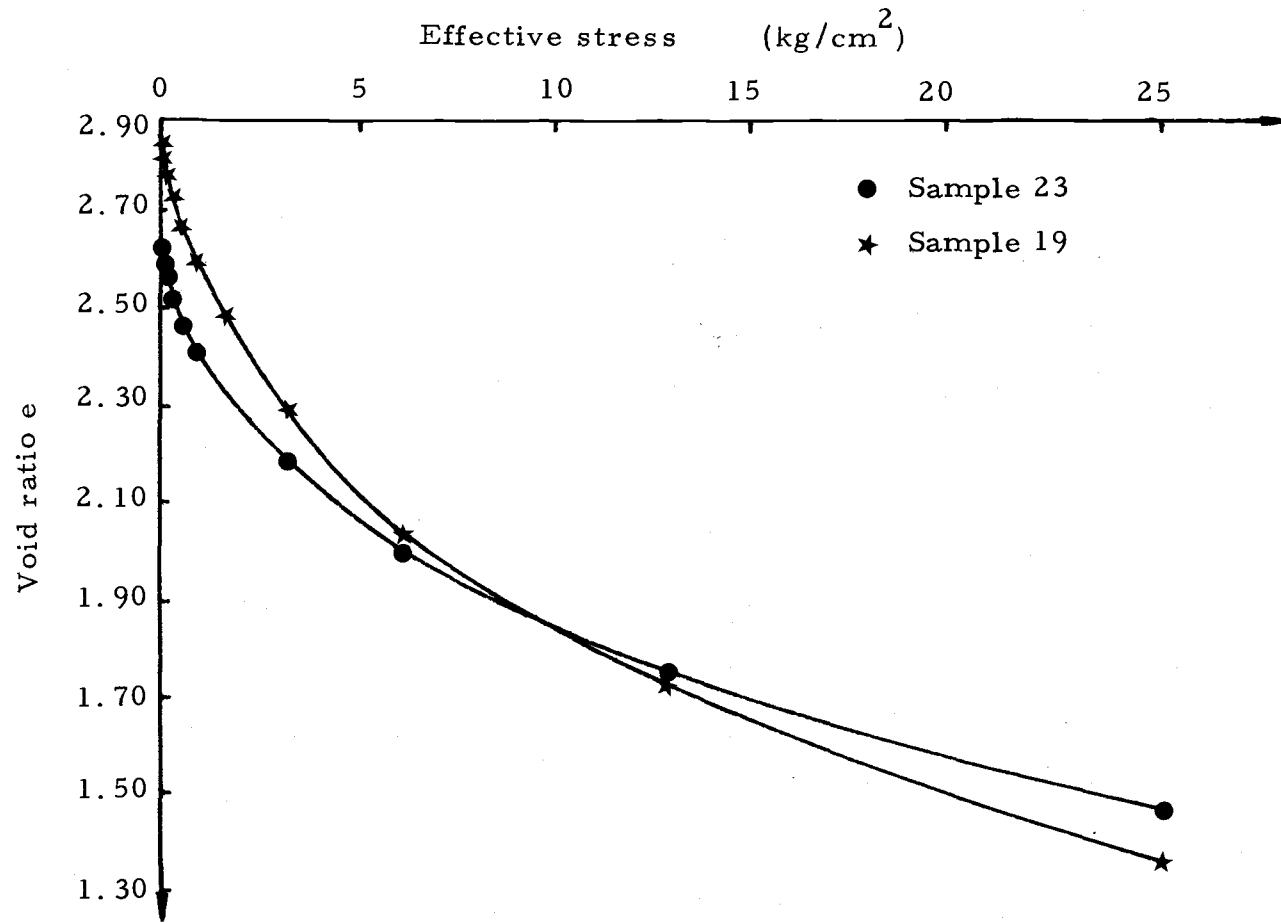


Figure 21. The void ratio vs effective stress curves of Samples 19 and 23.

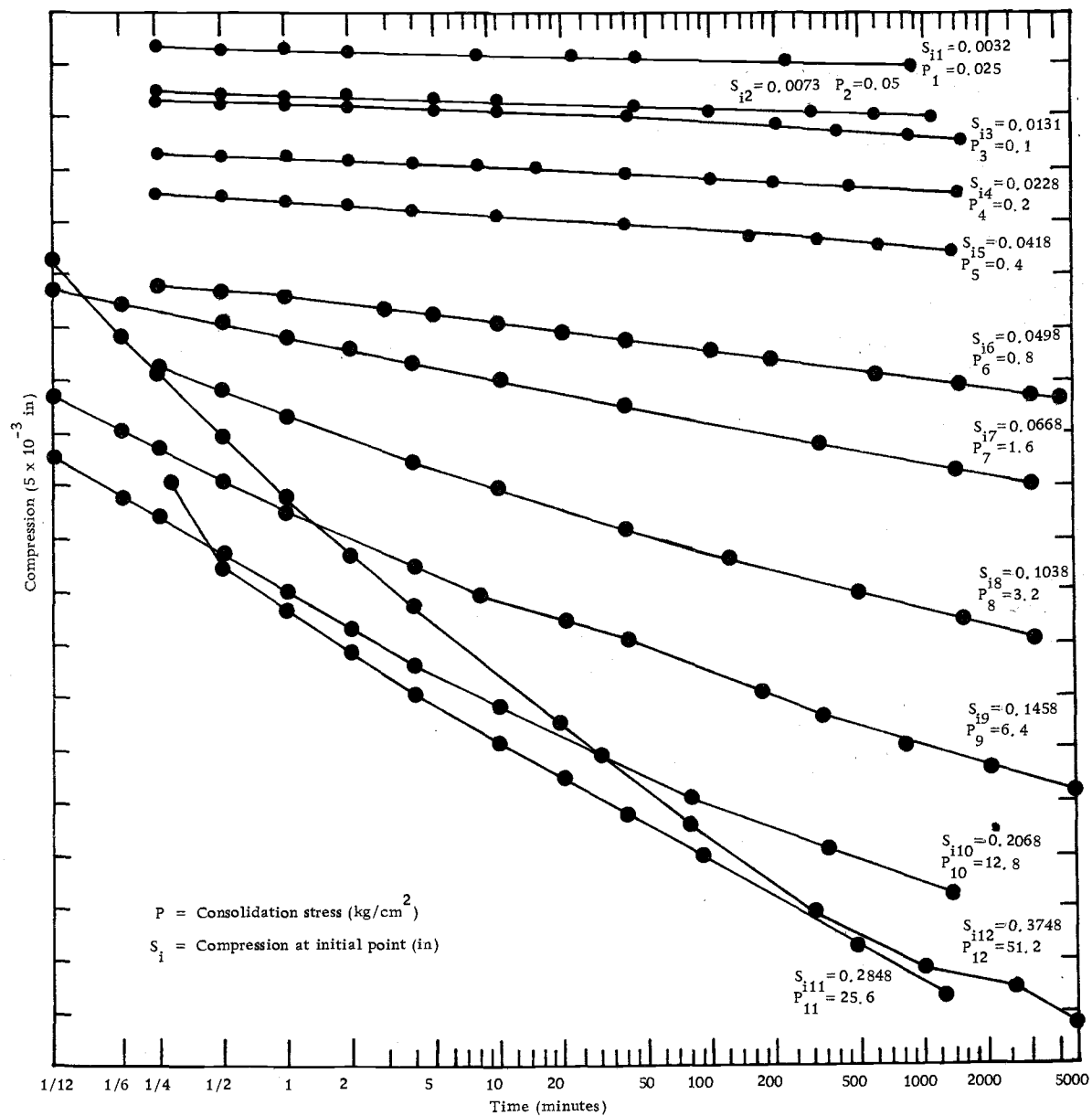


Figure 22. Time rate of consolidation curves of Sample 19.

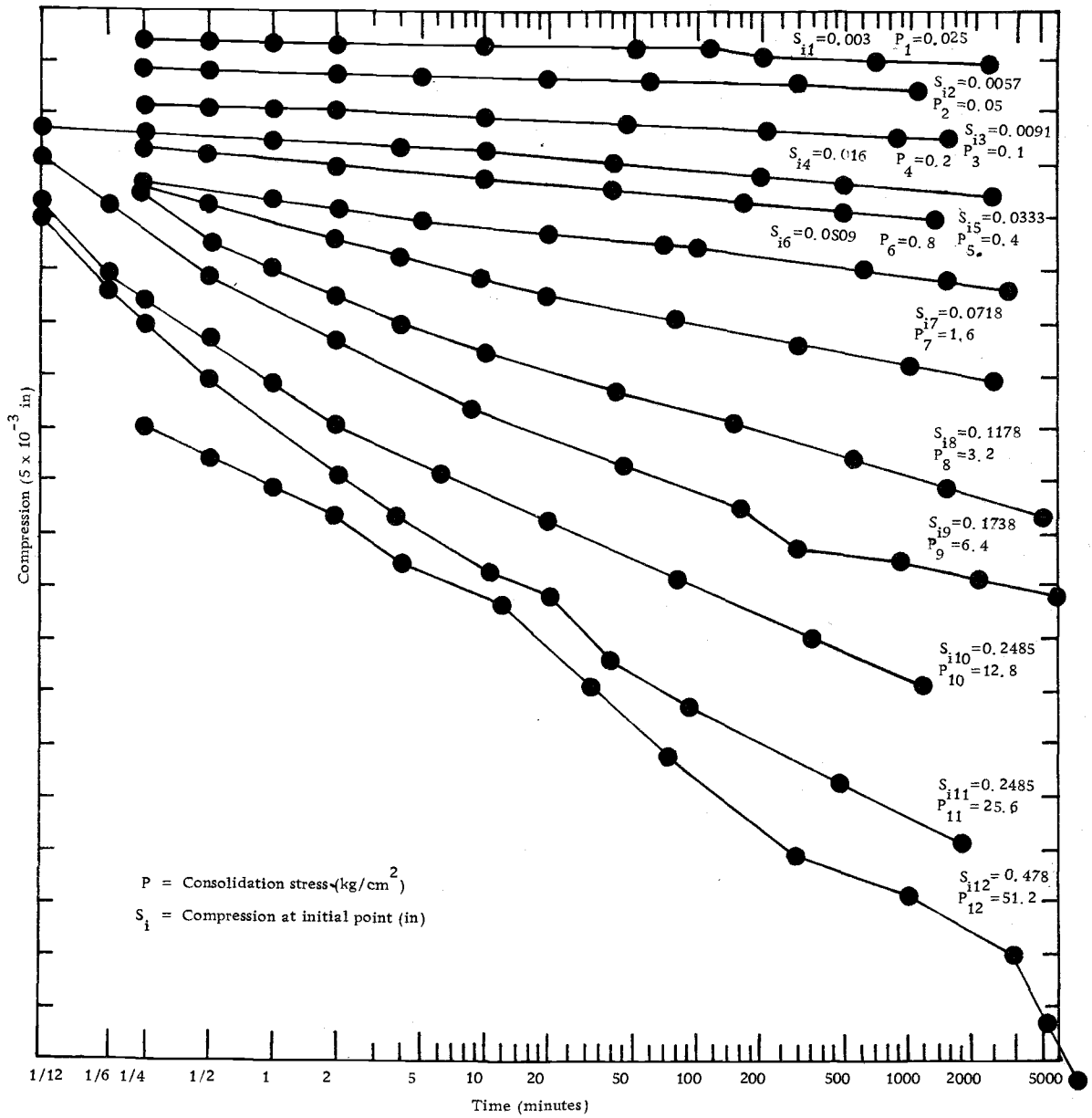


Figure 23. Time rate of consolidation curves of Sample 23.

DISCUSSION OF RESULTS

Five samples were used in the consolidation test (refer to Table 1). Owing to the limited amount of sample material, only Sample 12 at depth 912 cm and Samples 23 and 19 have been tested for determination of the Atterberg limits. Generally, in uniform soil, the samples obtained from the same short core should not differ much in plasticity. The low values of both the initial void ratio and the natural water content in Sample 12 at depth 912 cm were due to disturbance before the test. However, Sample 12 with depth 912 cm possessed a medium plasticity which could represent the soil properties of the other two samples with depth 135 cm and 446 cm. Sample 23 gave no value for the plastic limit test, and Sample 19 had a plastic index of 2. The test showed that Sample 12 may contain some percentage of clay, but there was no indication of the existence of clay in the other two samples. The latter two samples should have very similar consolidation characteristics. For reducing the influence of the clay content, Samples 19 and 23 have been considered as the basis for investigating the real soil behavior of calcareous sediments. In making a comparison between Figure 1 and the void ratio vs. effective consolidation stress curve (Figure 21) of foram soil, the stress-volume behavior of foram soil seems to fall mostly within the third stage derived by Lambe and Whitman. The continuous crushing of

the foram particles controlled most of the consolidation process.

Then comparing Figure 20 with Figure 21 the typical $e-p$ curves for soil which contains some percentages of mica have more or less the same shape as those of the foram sample. This indicates that scale-like particle content is one of the important factors of the consolidation characteristics of granular materials.

There are two series of time rate of consolidation curves representative of this soil (refer to Figures 21 and 22). Both showed a linear relationship between the compression and the elapsed time (log scale). They tend to become steeper with the increasing of consolidation stress. Temperature changes while testing may have produced some of the deviations on the time rate of consolidation curves. These time rates of consolidation curves indicate that secondary compression governed the consolidation. The linear relationship started at the fifth second and lasted up to 5000 minutes. The instantaneous settlement before the fifth second is hard to measure. There is no evidence that the rate of secondary compression will decrease even for intervals lasting over five days. After the foram tests start cracking under the increased pressure, there results a rapid dissipation of water followed by a gradual crushing of the particles. In the meantime, the crushing of grouped particles causes an overall uniform change in the settlement. Both sand (under high pressure) and foram particles have a very similar relationship

between compression and the logarithm of time (refer to Figures 10, 22 and 23). At the beginning of the consolidation test only a small amount of the particles were crushed. Either the progressive relaxation of cementation and bonding stress, or particle rearrangement controls the time lag and the initial settlement. Generally, in this test the time rate of consolidation attained a steady condition as the consolidation time reached the 60th minute, so the compressions at the 60th minute have been used to plot the void ratio-log effective stress curves. Five e -log p curves have been drawn here as Figures 19 and 20. All of them showed a common shape which is concave downward throughout the test. In other words, no straight line portion occurred on the e -log p curves, even at the highest consolidation stress of 52 kg/cm^2 . The sieve analyses (refer to Table 2) before and after testing show that the amount of particles which are larger than 0.074 mm in diameter has decreased about 50 percent in both Samples 19 and 23. The microscopic examination implied that the amount of fine particles has increased as a result of the consolidation. The evidence suggests that the continuous crushing of foram tests and the larger fragments is the main factor determining the concave downward e -log p curves without the straight line portion. The above phenomenon has also been found by the theoretical interpretation (refer to Figure 7).

On the basis of the test data presented, it appears that foram

sediments have an apparent overconsolidation stress even for the very shallow Sample 12, with a depth of 135 cm. There is no evidence that this deep sea sediment has had any overconsolidation. It may still be normally unconsolidated due to the gradually increasing deposition. The apparent overconsolidation stress probably reflects that some foram particles had been broken by the irregular impact of the bottom current of the ocean. Besides, some bonding stress probably resulted during the process of consolidation at the site and this may be another reason which might explain the apparent overconsolidation stress.

Another interpretation of the production of mineral cements runs as follows: Bottom-dwelling organisms produce CO_2 by respiration, which then dissolves to form carbonic acid. This carbonic acid reacts vigorously with the calcium carbonate contained in the foram tests so that Ca^{++} ions reacted with the carbonic acid again. Then calcium carbonate forms which mixes with the very fine soil and results in a slight cementation of the foram particles. The foram sediments have been observed by putting pieces of them into water, even after a period of two days they still were not deaggregated. Meanwhile, by storing the foram samples in a container for a period of two months to half a year, some thin white layers appeared surrounding the container. Perhaps the above phenomenon may be the indirect evidence for proving the existence of cementing material.

Up to now, unfortunately the secret of cementation still has not been exposed.

As mentioned before, the e - $\log p$ curves of the foram samples showed concave downward curves without a straight line portion. So the apparent overconsolidation stress is not easily found by using the conventional method. It was noted that the rate of secondary compression (C_a) increases with pressure to a maximum value and then starts decreasing under higher pressures. The peak value occurred at a value slightly higher than apparent overconsolidation stress (refer to Figure 11). Figure 24 is a plot of the rate of secondary compression against consolidation stress (log scale) for Samples 19 and 23. Both apparent overconsolidation stresses seem located at a value slightly lower than the stress of the first inflection point. Nevertheless, the apparent overconsolidation stress was still not distinct enough to be located easily. Results suggested that stress could be found by looking at the increments of the rate of secondary compression (ΔC_a). The arithmetic scale of the effective stress was plotted against ΔC_a , as shown in Figure 25. Samples 19 and 23 both had a first peak (lowest point shown on the graphs) and an apparent overconsolidation stress located at the first stress lower than the one of the maximum ΔC_a . A possible explanation is that the cementation or bonding stress starts to break at the apparent overconsolidation stress. Beyond this stress a great increase occurs

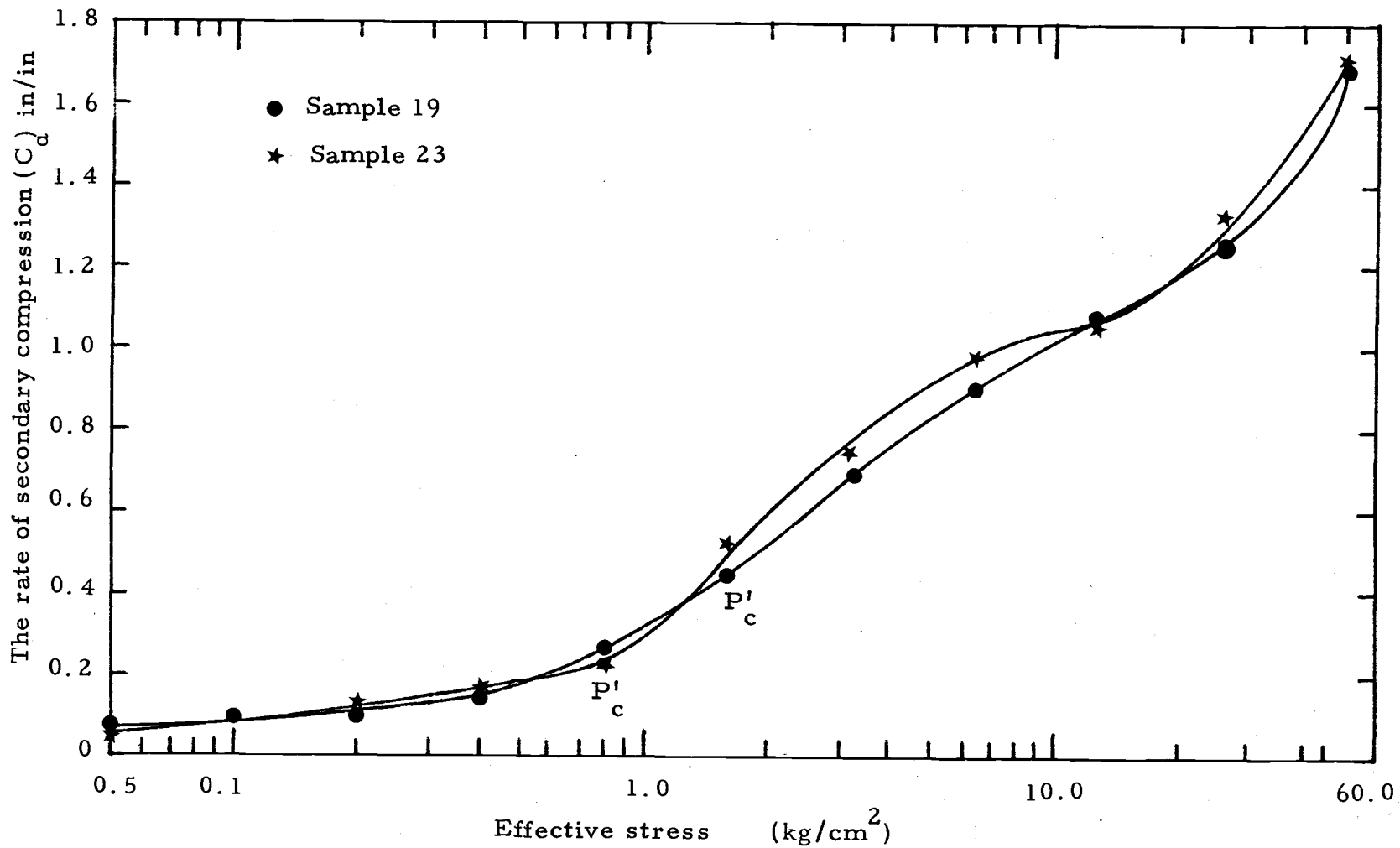


Figure 24. Effective stress vs the rate of secondary compression curves

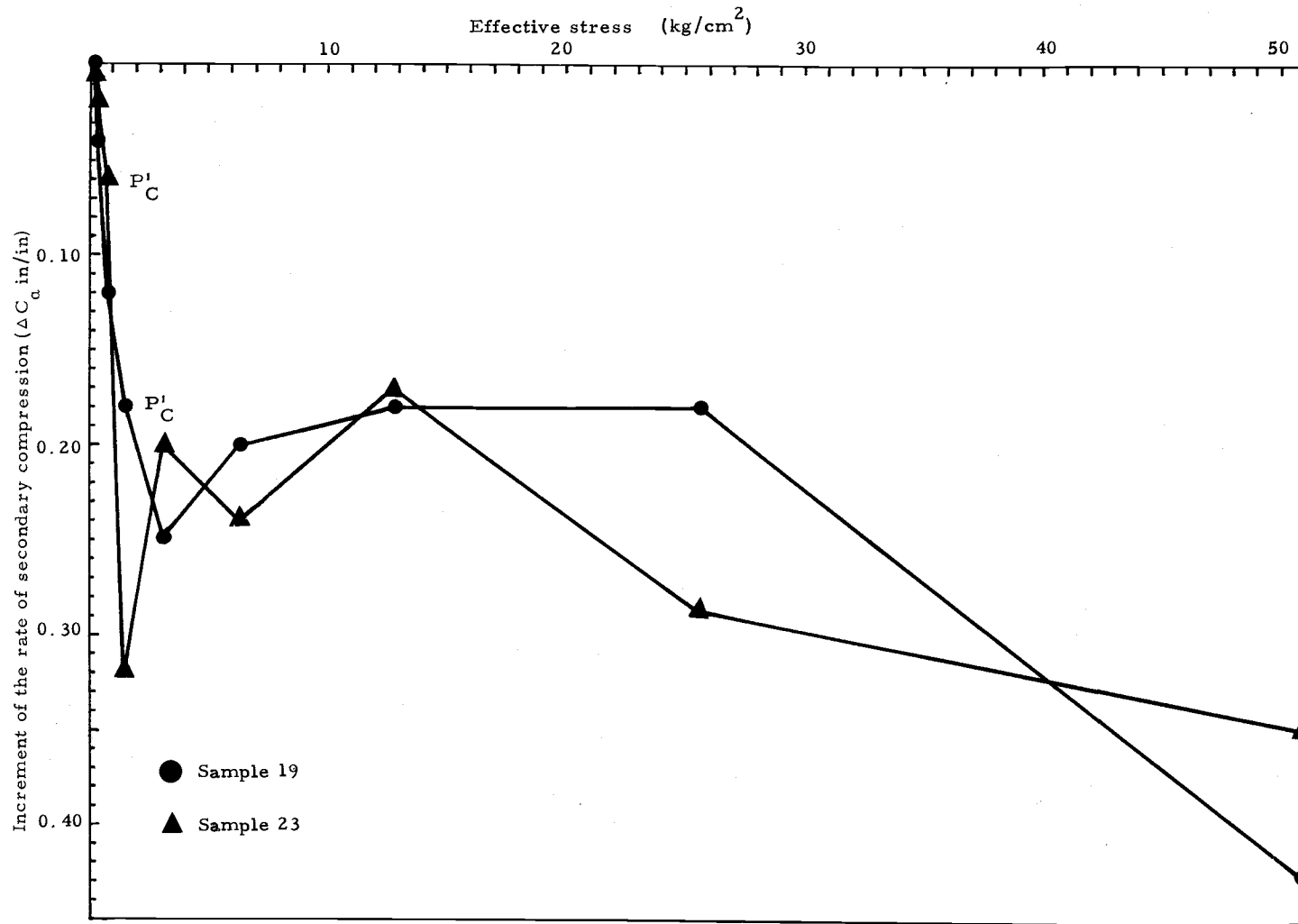


Figure 25. Effective stress - increment of the rate of secondary compression.

on the slope of the time rate curve at the next higher load because of the relaxation of the particles from bondage. Above the stress at the peak point, the increment of secondary compression (ΔC_a) starts to change irregularly. A comparison was made between Figures 11 and 24, and the difference between these curves may be caused by difference in clay content. The soil represented in Figure 11 is a clayey silt. The peak point in $C_a - \log p$ curves probably will not exist in hollow-size particles. The variations in apparent overconsolidation stress versus depth have been shown in Figure 26. The apparent overconsolidation stress first increases with depth, and then approaches a constant. If cementation happens in the foram sediments, the stress (P'_c) may remain constant below a certain depth. Above that depth, cementation increases with the depth. In other words, the degree of cementation correlated with the increase in time. The longer the sediments form, the greater is the cementation. As cementation reaches a limiting value, it will maintain a constant value regardless of a continued increase in time.

As previously mentioned, the three-range theory has been used in this paper to demonstrate the consolidation characteristics of foram sediments. Microscopic examination of foram particles revealed that the ratio of internal to external diameter (R) was found to be about 8:9. Therefore, the initial internal and external void ratio (e_{ino} , e_{out}) were determined to be

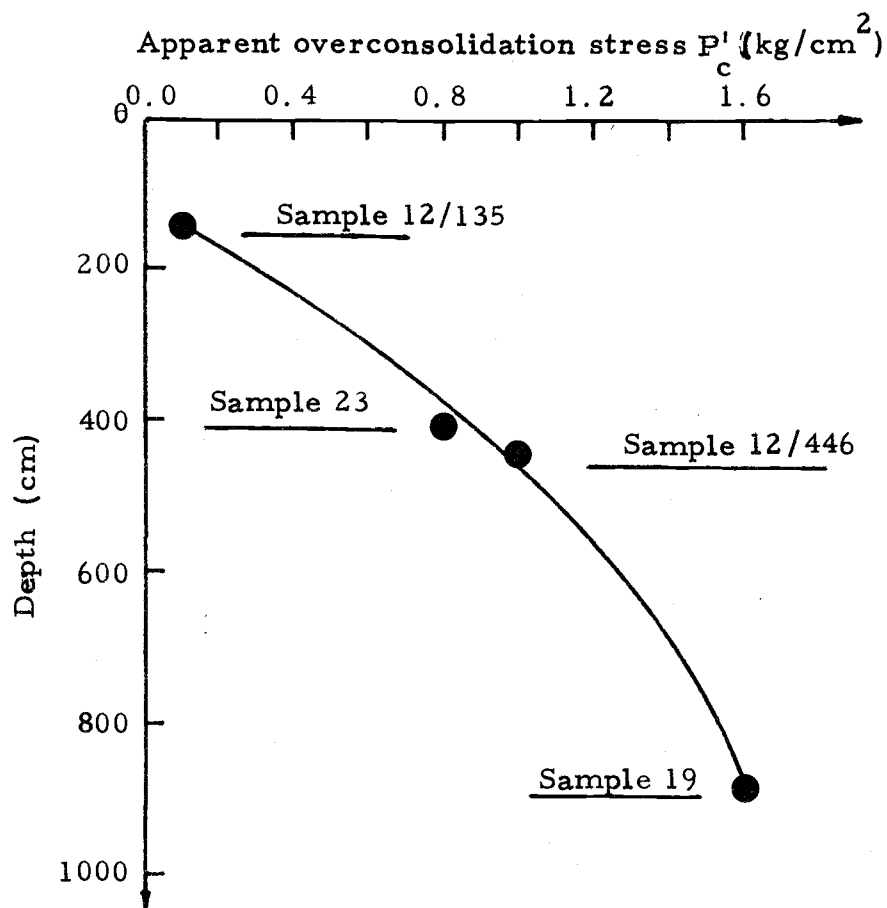


Figure 26. The variation between apparent overconsolidation stress and depth (below ocean bottom)

$$e_{ino} = \frac{R^3}{1-R^3} = 2.36$$

$$e_{out} = \frac{0.275}{1-(R^3)} = 0.91$$

Therefore, the total void ratio was

$$e_o = e_{ino} + e_{out}$$

$$e_o = 0.91 + 2.36 = 3.27$$

Substitute above values into Equation (7). The relationship between compression index and void ratio was established as follows

$$C_{cm} = \left(\frac{3.27 - e}{2.36} \right) C_{cf} \quad (10)$$

Based upon this equation, Figure 8 can be refined as Figure 27.

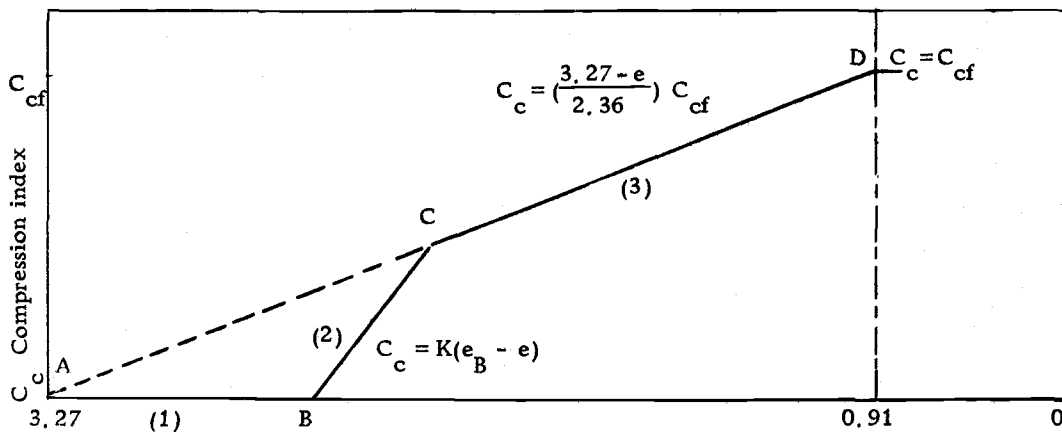


Figure 27. The refined interpretation of the correlation between the compression index and void ratio

Based upon the theory, then, the compression index is a function of void ratio. By using this approach, Figure 28 represents the results of the investigation of Samples 19 and 23 and plotted as compression index (C_c) vs void ratio (e). The results of these two samples show satisfactory agreement. The agreement is probably a result of similar soil properties. The Atterberg limit has not indicated any clay content in these two samples, so in these two samples the soil behavior was mostly controlled by the foram particles. Therefore their results are probably characteristic of the calcareous sediments. To compare these results with the refined theoretical interpretation in Figure 25, a conformity in the relationship of compression index and void ratio was shown. Three distinct ranges appear in the results. The main relationship lines of Samples 19 and 23 are all extended to the origin point, which has a void ratio of 3.27. This value is in agreement with the estimated initial total void ratio (e_o). The first range is located from 3.27 to about 2.77. Second range was approximately between 2.77 and 2.19. The slope of C_c - e line is 1.40, so the representative equation is

$$C_{cm} = 1.40 (e_B - e)$$

$$C_{cm} = 1.40 (2.77 - e) \quad (11)$$

Results suggest that after the void ratio becomes less than

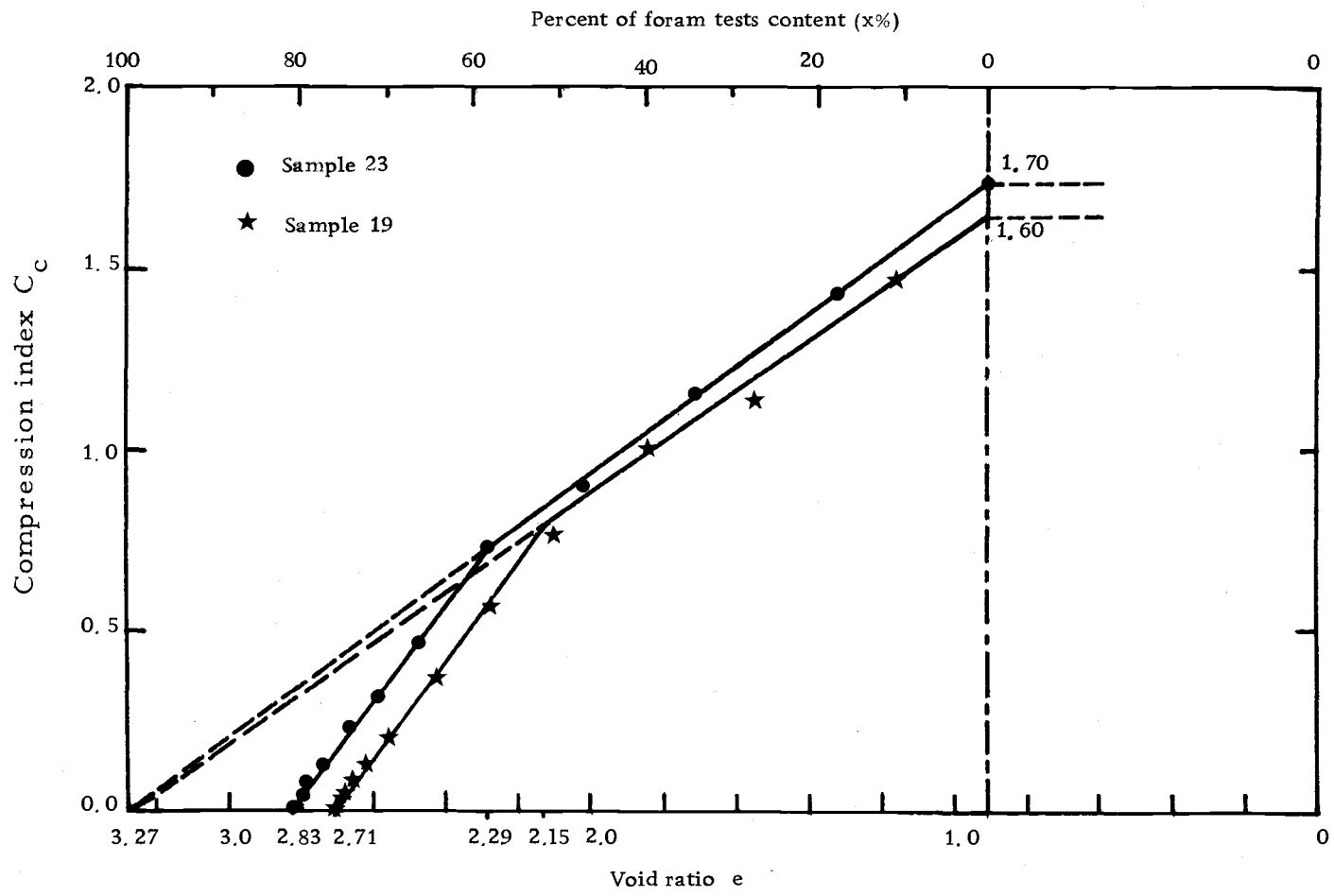


Figure 28. The relationship between the compression index and void ratio (from consolidation results)

0.91, all the foram test had been crushed to fragments and an unchanged compression index occurred on the e -log p curve. Sample 23 had been consolidated to a void ratio about 0.91, so it was used to check whether or not all the foram tests became fragmented. As sieve analyses and microscopic examination indicated, the particles passing through the No. 200 sieve were composed of crushed fragments only, but the particles retained on sieve No. 100 and No. 200 were composed of both foram tests and fragments. After the consolidation test on Sample 23, 8.5 percent and 9.9 percent foram particles were retained on sieves No. 100 and No. 200 respectively. The microphotographs show that about 18 percent and 5 percent foram tests appear among the particles which were respectively retained on the No. 100 and No. 200 sieves. Summarily, there were approximately 98.0 percent fragments in Sample 23 after the test. Result from the consolidation test of Sample 23 gives a theoretical value of 100 percent foram tests when the void ratio reaches 0.91. The error between the theoretical approach and the grain size analysis is about 2 percent. This reasonable agreement implies that the external void ratio 0.91 could be considered a boundary for the existence of foram tests and fragments.

After passing this boundary, the compression index may maintain a constant C_{cf} value for a short interval as the void ratio decreases. The average value of the compression index (C_{cf}) from

the consolidation of Samples 19 and 23 was about 1.65 (refer to Figure 28). The compression index-void ratio equation in the third range was rewritten as follows (refer to Equation 10).

$$C_{cm} = \left(\frac{3.27 - e}{2.36} \right) 1.65$$

$$C_{cm} = 0.7 (3.27 - e) \quad (12)$$

This equation is valid, as the void ratio is located between 2.19 and 0.91. To compare Equations 11 and 12, the slope of the compression index-void ratio $C_c - e$ line in the second range was double its value in the third range.

Based upon the above findings the three ranges could also be regarded in terms of the percentage of foram tests or fragments. Above 79 percent foram test, the compression index became zero, i. e., the foram tests control the system's behavior. The transition zone is located from 79 percent to 54 percent foram test content. Beyond this zone, fragments dominated soil behavior. As mentioned in the theory, the transition zone is interpreted to be between 50 percent and 71 percent foram test content. This reasonable agreement of findings suggests that there is a transition range in the hollow matrix of foram particles.

CONCLUSIONS

1. There are four important factors which significantly influence the consolidation characteristics of calcareous sediments:
(1) initial void ratio, (2) scale-type particles content, (3) clay soil content, and (4) foram tests content.
2. The consolidation characteristics of the calcareous samples tested are independent of the load increment ratio.
3. Test results established the fact that the e -log p consolidation curves maintain a concave downward shape throughout the stress range tested without a straight-line portion.
4. The calcareous sediments tested have an apparent overconsolidation stress higher than the in situ stress even in samples from shallow depth. The apparent overconsolidation stress is not easily found by using the conventional method. Results suggest that this stress may be found from a curve of the consolidation stress vs the increment of the rate of secondary compression (ΔC_{α}). The apparent overconsolidation stress is located at the first stress lower than the one having the maximum increment of secondary compression (ΔC_{α}). The apparent overconsolidation stress appears to increase with depth at a decreasing rate.
5. For sediments which initially consist solely of whole foram tests, the theoretical relationship between the compression index and

the void ratio has three distinct ranges. The first range is dominated by foram test crushing and has a very small compression index ($C_c \approx 0$). The second range is a transition stage and is defined by $C_c = 1.4 (2.77 - e)$. The third zone is controlled by the compression of the foram fragments. In this range as void ratio and percentage of whole tests decrease, more fragments are produced and the compression index increases in proportion to the amount of fragments. In the third range $C_c = 0.7 (3.27 - e)$.

RECOMMENDATIONS FOR FUTURE STUDY

There are three possible causes for the occurrence of apparent overconsolidation stress: (1) the interparticle bonding strength, (2) cementation, and (3) particle crushing by the irregular impact of the bottom current of the ocean. Although most investigators have postulated that cementation may occur in calcareous sediments, nobody has proven it. Research on this area should be emphasized in future studies.

The scope of the relationship established during this study has been limited by the equipment, for the pressure used in the test could reach a maximum of only 52 kg/cm^2 . As the pressure reaches a rather high value, overall fine fragments will characterize the sample and there could be a straight line portion on the e -log p consolidation curve. There is probably a corresponding compression index for every foram sample if the factor of clay content has been modified. If a greater load were applied to the selected samples, the above phenomena probably could be proven. Further studies on the detailed physical properties of the foram particles should be made in order to find a more accurate theoretical approach to the study of consolidation characteristics.

BIBLIOGRAPHY

1. American Association of State Highway Officials. Standard specifications for highway materials and methods of sampling and testing. Part II, 10th edition, Washington, D.C. 1970.
2. American Society for Testing and Materials. Procedures for testing soil. ASTM Committee D-18, Philadelphia. 1964.
3. Anderson, D.G. Consolidation characteristics of sand-clay mixtures. Master's thesis. Corvallis, Oregon State University, 1968. 47 numb. leaves.
4. Forouki, Omar T. and Hans F. Winterkorn. Mechanical properties of granular systems. Highway Research Record 52:10-42. 1964.
5. Gilboy, Glennon. The compressibility of sand-mica mixtures. Proceedings of the American Society of Civil Engineers 54:555-573. 1928.
6. Lambe, T.W. and Robert V. Whitman. Soil mechanics. New York, John Wiley and Sons, 1969. 533 p.
7. Murdock, L.J. Consolidation tests on soils containing stones. In: Proceedings of the Second International Conference on Soil Mechanics and Foundation Engineering, Rotterdam, 1948. Vol. 1. Rotterdam. p. 169-173.
8. Oglesby, Clarkson H. and Laurence I. Hewes. Highway engineering. 2d ed. New York, John Wiley and Sons, 1963. 783 p.
9. Roberts, J.E. and J.M. deSouza. The compressibility of sand. Proceedings of the American Society for Testing Materials, 1958. Vol. 58. p. 1269-1277.
10. Sing, A. and Zan Yang. Secondary compression characteristics of a deep ocean sediment. Proceedings of the International Symposium on the Engineering Properties of Sea-floor Soils and Their Geophysical Identification. Sponsored by UNESCO, National Science Foundation and University of Washington, 1971, p. 121-129.

11. Sowers, George B. and George F. Sowers. Introductory soil mechanics and foundations. New York, The Macmillan Co., 1961. 386 p.
12. Taylor, D. W. Fundamentals of soil mechanics. New York, John Wiley and Sons. 1948, 217 p.
13. Terzaghi, K. and R.B. Peck. Soil mechanics in engineering practice. New York, John Wiley and Sons. 1967. 729 p.